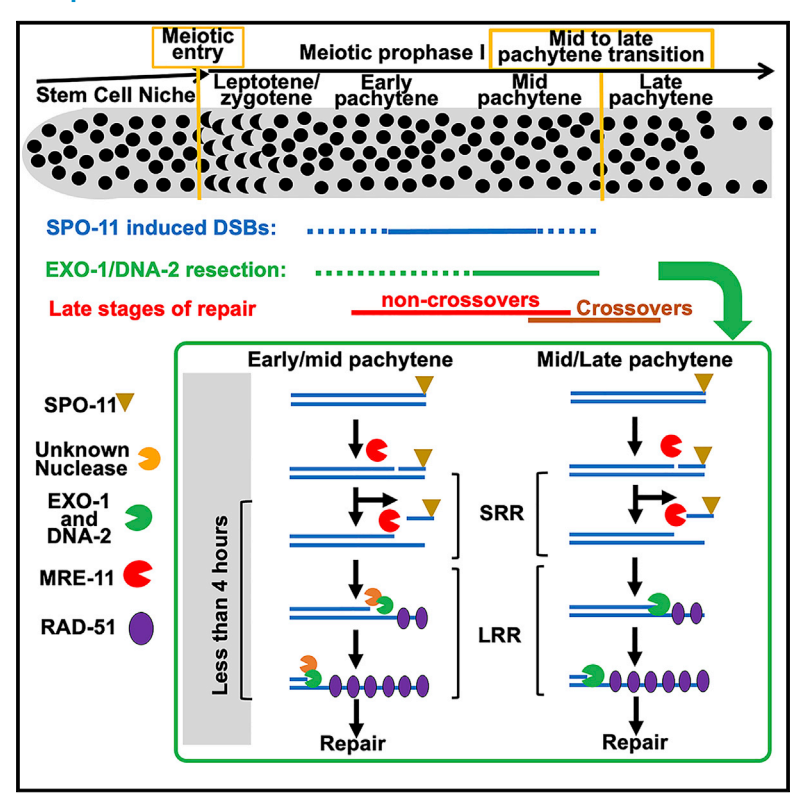
Continuous double-strand break induction and their differential processing sustain chiasma formation during Caenorhabditis elegans meiosis

Graphical abstract



Authors

Tara Hicks, Shalini Trivedi, Mikayla Eppert, ..., Caroline Crahan, Sarit Smolikove, Nicola Silva

Correspondence

sarit-smolikove@uiowa.edu (S.S.), silva@med.muni.cz (N.S.)

In brief

Meiotic chromosome segregation requires Spo11-mediated break induction and long end resection to form crossovers. Hicks et al. show that break formation occurs throughout pachytene stage in *C. elegans*, and those formed later are essential to generate crossovers. DNA-2/EXO-1 activity mainly on later breaks ensures homologous recombination-dependent repair, preventing non-homologous end joining.

Highlights

- Meiotic DSBs are formed continuously throughout the pachytene stage in C. elegans
- DSBs formed at later meiotic stages are essential to generate crossovers
- The nucleases DNA-2 and EXO-1 resect DNA ends predominantly at later meiotic stages
- DNA-2/EXO-1 activity discourages non-homologous endjoining-dependent repair







Article

Continuous double-strand break induction and their differential processing sustain chiasma formation during *Caenorhabditis elegans* meiosis

Tara Hicks, Shalini Trivedi, Mikayla Eppert, Richard Bowman, Hui Tian, Amna Dafalla, Caroline Crahan, Sarit Smolikove, and Nicola Silva^{2,3,*}

SUMMARY

Faithful chromosome segregation into gametes depends on Spo11-induced DNA double-strand breaks (DSBs). These yield single-stranded 3' tails upon resection to promote crossovers (COs). While early Mre11-dependent end resection is the predominant pathway in most organisms, Exo1 or Dna2/BLM can also contribute to the efficient processing of meiotic DSBs. Although its enzymatic activity has been thoroughly dissected, the temporal dynamics underlying Spo11 activity have remained mostly elusive. We show that, in *Caenorhabditis elegans*, SPO-11-mediated DSB induction takes place throughout early meiotic prophase I until mid-late pachynema. We find that late DSBs are essential for CO formation and are preferentially processed by EXO-1 and DNA-2 in a redundant fashion. Further, EXO-1-DNA-2-mediated resection ensures completion of conservative DSB repair and discourages activation of KU-dependent end joining. Taken together, our data unveil important temporal aspects of DSB induction and identify previously unknown functional implications for EXO-1-DNA-2-mediated resection activity in *C. elegans*.

INTRODUCTION

Sexual reproduction relies on the generation of haploid gametes through meiosis, a highly regulated cell division mechanism essential for the faithful transmission of the genetic information across generations (Zickler and Kleckner, 1999, 2015). A crucial and unique aspect of meiosis is the programmed formation of DNA double-strand breaks (DSBs) carried out by the topoisomerase-like Spo11 (Keeney et al., 1997). These DSBs are in turn resected to generate 3' overhanging tails, which are ultimately loaded with Rad51/RecA to promote inter-homolog recombination-mediated repair (HR) to yield crossovers (COs) (Borde, 2007). COs act as a physical tether between each pair of homologs conferring the required tension upon which the forces of the spindle fibers will exert their pulling action, eliciting migration of one homolog to each cell pole. Failure in DSB formation prevents execution of HR and consequently absence of COs, thereby producing aneuploid gametes due to random chromosome segregation (Dernburg et al., 1998; Keeney et al., 1997).

In most organisms, MRX/N complex (Mre11-Rad50-Xrs2/Nbs1)-dependent resection occurs as an early event during meiotic DSB processing and is required for the removal of Spo11-DNA covalent adducts (Stracker and Petrini, 2011). Since Mre11 cuts in proximity to Spo11, this is proposed to generate short overhangs not sufficient for the execution of HR. Work in yeast established that these short-range resection tracts are

expanded to form long single-stranded DNA (ssDNA) by the long-range resection (LRR) nucleases; predominantly by Exo1, with some involvement of Dna2/BLM (Garcia et al., 2011; Manfrini et al., 2010; Zakharyevich et al., 2010). In metazoans, Exo1 was shown to play a minor role in meiotic resection, and identifying a role for Dna2 was challenging due to its essential role during replication (Paiano et al., 2020; Yamada et al., 2020). In *Caenorhabditis elegans*, MRE-11 is required for both the induction and resection of meiotic DSBs (Chin and Villeneuve, 2001; Yin and Smolikove, 2013), while EXO-1 is dispensable for accurate DNA repair and establishment of COs but holds more important roles in the absence of MRE-11-dependent resection activity (Yin and Smolikove, 2013).

Importantly, while pro-DSB co-factors have greatly diverged throughout evolution, Spo11 is instead highly conserved, and its enzymatic activity is essential to generate DSBs across species. Spo11-DNA complexes can be biochemically pulled down and further processed to identify cutting sites in plants, yeast, and mice models, describing in great detail the molecular mechanisms through which Spo11 exerts its activity (Johnson et al., 2021; Lam et al., 2017; Lange et al., 2016; Prieler et al., 2021). However, detection of this protein has proved difficult in different model systems, and only in a few studies has cytological detection of SPO11 foci or localization along the chromosome axes been shown (Choi et al., 2018; Romanienko and Camerini-Otero, 2000; Vrielynck et al., 2021).



¹Department of Biology, The University of Iowa, Iowa City, IA 52242, USA

²Department of Biology, Faculty of Medicine, Masaryk University, Brno 625 00, Czech Republic

³Lead contact

^{*}Correspondence: sarit-smolikove@uiowa.edu (S.S.), silva@med.muni.cz (N.S.) https://doi.org/10.1016/j.celrep.2022.111403



Previous work in C. elegans revealed that pro-DSB co-factors DSB-1-3 can be cytologically detected from transition zone to mid-pachytene stage, and that they respond to impaired CO formation by extending chromatin competency in undergoing DSB formation (Hinman et al., 2021; Rosu et al., 2013; Stamper et al., 2013). However, these proteins are also extensively loaded in DSB-deficient backgrounds (i.e., spo-11 and him-17 nulls), indicating that, while presumably operating in a "checkpoint"-like fashion, they cannot be considered as a direct readout of DSB execution per se. Moreover, other pro-DSB players, such as HIM-17, XND-1, and MRE-11, are robustly loaded throughout the gonad, including the pre-meiotic tip and the nucleoplasm of diplotene and diakinesis cells (Janisiw et al., 2020; Reddy and Villeneuve, 2004; Wagner et al., 2010), where no DSBs are present. Thus, the localization of these proteins does not necessarily overlap with break formation, and temporal assumptions about DSB induction cannot be inferred from cytological localization of these factors.

In many species, SPO11 is required for chromosome synapsis, and Spo11 mutants exhibit meiotic arrest. Specifically, mice mutants fail to progress beyond zygotene stage during spermatogenesis (Romanienko and Camerini-Otero, 2000), indicating that DSBs must be generated before pachytene entry to successfully complete SC installation and meiotic progression. However, these data do not disprove a model by which meiotic DSBs are formed continually, and into later stages of meiosis. Indeed, recombination intermediates (Dmc1/Rad51 labeled) are gradually recruited throughout pachytene in many species, suggesting that DSBs may be generated in later stages of meiosis as well (Bishop, 1994; Kauppi et al., 2013; Mets and Meyer, 2009; Roig et al., 2010; Sanchez-Moran et al., 2007; Thacker et al., 2014). However, since DSB repair may not be synchronous, these lingering intermediates may also reflect a delay in DSB repair (Joshi et al., 2015), leaving the window of DSB formation ambiguous.

By employing a functional auxin-inducible degron (AID)-tagged line, we provide evidence that, during C. elegans meiosis, SPO-11mediated DSBs occur at multiple times during meiotic progression, bearing different functional implications for CO formation. Our data are consistent with a wave of DSBs produced at meiosis entry (transition zone); however, generation of breaks does not halt as cells enter early pachytene stage but, rather, they are continuously formed until mid-late pachytene stages. Moreover, we found that DNA breaks formed at later stages are a substrate for EXO-1-DNA-2-mediated resection, which acts redundantly to ensure that processing of DSBs is efficiently accomplished to successfully form inter-homolog COs and prevent activation of canonical non-homologous end-joining (cNHEJ). Taken together, our work provides major insights into understanding SPO-11 activity in metazoans and further illuminates the resection-mediated processing of meiotic DNA breaks in nematodes.

RESULTS

SPO-11 mediates DSB induction at early and later stages of meiotic prophase I

The C. elegans gonad is organized as a syncytium, in which multiple nuclei share a common cytoplasm. The distal portion of the

gonad contains progenitor cells, which continuously divide before entering meiosis. Meiocytes are synchronized in the different stages of meiotic prophase I and proceed through the gonad at a pace of roughly one cell row per hour, allowing the analysis of meiotic events with precise spatiotemporal resolution (Figure 1A) (Hillers, 2017; Jaramillo-Lambert et al., 2007). Further, thanks to easy exploitation of the AID system in worms, it is possible to modulate the depletion of endogenous proteins at different time windows to assess differential, stage-dependent roles exerted by these factors (Zhang et al., 2015).

We employed an available functional spo-11::AID::3xFLAG line to unravel the temporal dynamics of SPO-11 activity within the germ line (Zhang et al., 2018). This line has been shown to be functional, as, unlike spo-11 null mutants, it displays normal levels of fertility and no defects in the establishment of chiasmata. However, (1) we wanted to rule out that the spatiotemporal progression of the meiotic germ cells in the gonad was not altered compared with untagged wild-type controls, and, further, (2) we wished to compare the progression rate in worms staged as L4 or young adult when exposed to auxin started, since it has been previously shown that the pace of nuclear progression changes in an age-dependent manner (Jaramillo-Lambert et al., 2007; Tolkin and Hubbard, 2021). To this end, spo-11::AID::3xFLAG and wild-type worms were given a short pulse of 5-Ethynyl-2'-deoxyuridine (EdU) (see STAR Methods) and then placed on auxin-containing plates for 20 and 40 h. Detection of EdU-labeled cells revealed no major differences between the spo-11::AID::3xFLAG and the untagged animals exposed to auxin, as the percentage of cell rows traveled within the germ line was nearly identical in the two backgrounds (Figures 1B-1D) and, importantly, it recapitulated previous data (Almanzar et al., 2022; Jaramillo-Lambert et al., 2007). We observed a similar, slightly reduced pace in the L4 spo-11::AID::3xFLAG animals exposed to auxin for 40 h or young adults treated for 20 h (~10%), and, although they are statistically significant, these differences are unlikely to bear any biological relevance, given that in both cases they encompass nuclei localized within the same stage.

Having assessed that neither the genetic background, age, nor the exposure to auxin have a major impact on the oocytes' progression, we proceeded to investigate the temporal dynamics underlying SPO-11-mediated DSBs by analyzing the loading of the recombinase RAD-51, since a direct marker for DSBs in worms is currently lacking. RAD-51 has been shown to engage/disengage from the chromatin with comparable expression profiles across a multitude of studies, although the average number of foci/nucleus is subject to some differences due to different operators/staining protocols, as well as anti-RAD-51 antibodies employed in the field.

Short pulses of 1 h exposure to auxin sufficed to elicit disappearance of roughly half of the chromatin-associated RAD-51 foci throughout early to mid-pachytene stage in the *spo-11::AID::3xFLAG* worms (Figure 2A, zones 3–5), and additional exposure to auxin for 2 and 4 h, further reduced RAD-51 foci formation throughout the gonad (Figures 2A, S1A, and S1B). We also performed exposure to auxin for longer times (13 and 24 h), which only had a minor impact in further abrogating RAD-51 detection and suggesting that depletion of SPO-11 for as little

Cell Reports Article



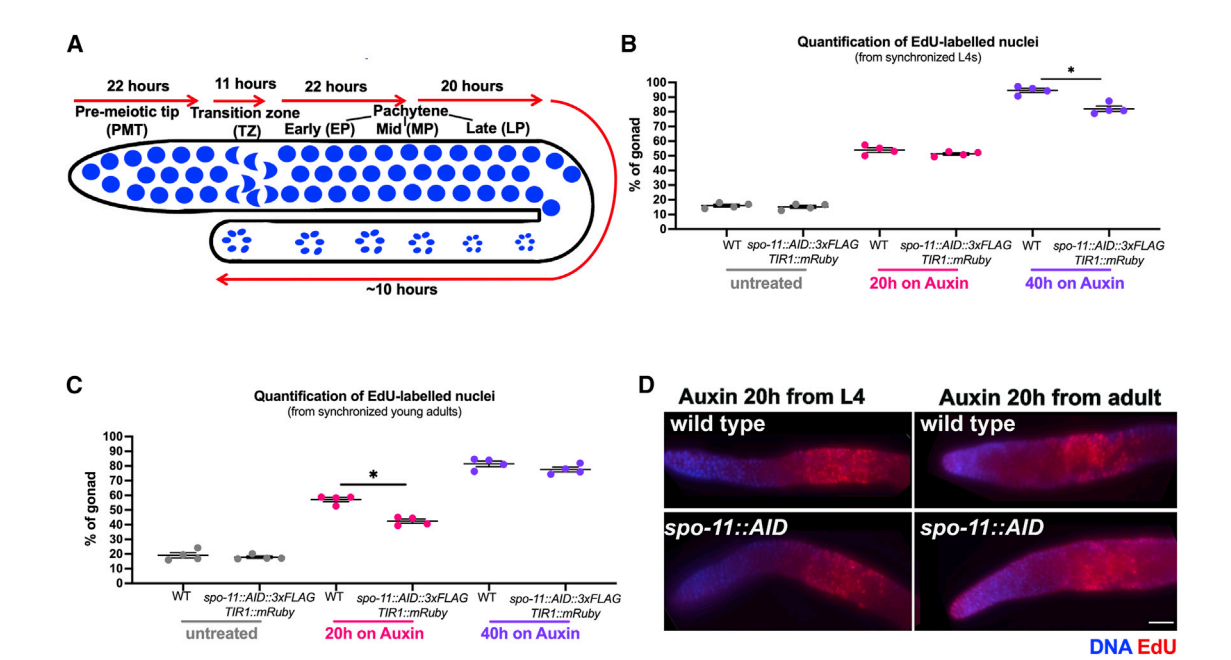


Figure 1. Response to auxin is independent of age

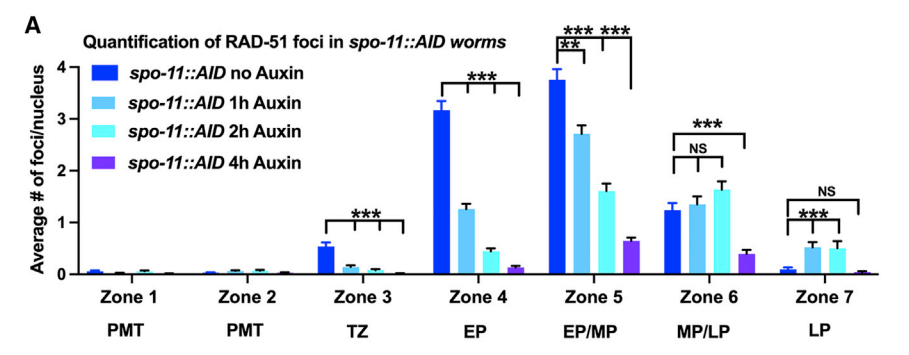
- (A) Schematic representation of spatiotemporal progression of the germ cells in the gonad.
- (B) Age-matched worms exposed to auxin as L4s for different time windows display similar nuclear progression.
- (C) Age-matched worms exposed to auxin as young adults (1 day post L4) for different time windows display similar nuclear progression. The x axes in (B) and (C) represent the furthest position of the EdU-positive row divided by total number of nuclear rows.
- (D) Representative images of EdU-stained gonads from differently staged animals at the indicated times. Scale bar, 20 µm, All analyses were performed in at least three gonads and in biological replicates. Data are shown as mean \pm SD. Asterisks indicate p < 0.01 as calculated by Mann-Whitney test.

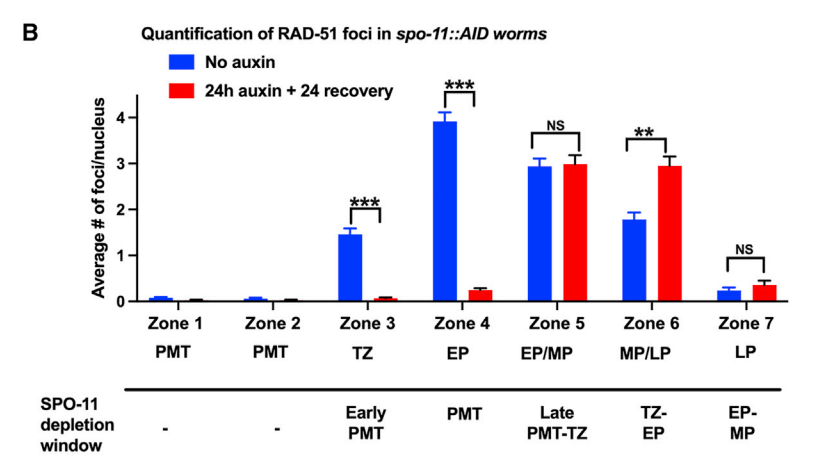
as 4 h is enough to nearly fully abrogate RAD-51 loading (Figure S2A). We reasoned that, if DSBs were only induced at early meiosis onset, then we would have expected a disappearance of RAD-51 only between transition zone and early pachytene, whereas the fact that we found a dramatic reduction of foci within only 4 h of exposure to auxin soundly corroborates that DSB induction is an extended spatial process that undergoes rapid processing. Therefore, the global impairment of foci that we observe is more consistent with a broader window of SPO-11 activity. Given that meiocytes progressed in the gonad only for 1-4 h during the AID-induced depletion (roughly four cell rows in total), we can infer that DSBs are generated across the whole pachytene stage. Importantly, we monitored RAD-51 focus formation in identically treated wild-type animals, which showed negligible effects (Figure S2C), ruling out possible artifacts due to the presence of auxin and confirming that reduced detection was solely due to SPO-11 removal.

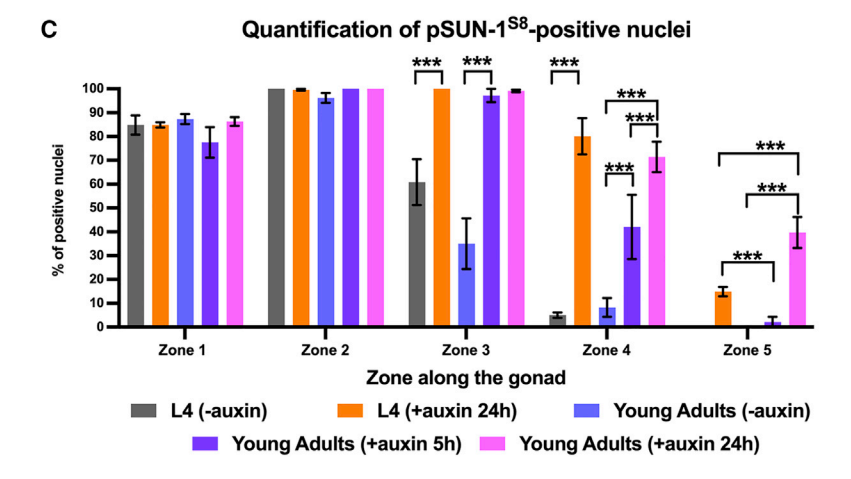
We also performed a recovery experiment, in which we exposed the spo-11::AID::3xFLAG worms to auxin for 24 h and then we allowed them to grow further for 24 h on plates without auxin. Analysis of RAD-51 shows that, in nuclei where the SPO-11 depletion had occurred at early meiosis onset (transition zone-early pachytene), abundant foci are detectable (Figure 2B, zones 5 and 6, and Figure S2B), while, surprisingly, we did not observe a clear recovery of RAD-51 at earlier stages (zones 3-4). This could suggest that the nuclei residing in the pre-meiotic tip during depletion may fail in generating the recombination intermediates as SPO-11 loading could be promoted right before entering the transition zone. These results imply that SPO-11 licensing requires passage through mitosis (see section "discussion"). To test whether SPO-11 is recruited to DNA in mitotic nuclei, we attempted to cytologically localize SPO-11::3xFLAG and we also generated a functional spo-11::HA by CRISPR-Cas9, but we were not successful in either case at visualizing SPO-11 (Figure S3A).

Failure in DSB formation or homologous recombination elicits activation of a surveillance system that detects unfinished meiotic tasks and triggers extended phosphorylation of the nuclear envelope component SUN-1, prolonging a DSB-competent state (Rosu et al., 2013; Stamper et al., 2013; Woglar et al., 2013) by delaying removal of pro-DSB co-factors DSB-1/2/3 from the chromatin. We sought to monitor the checkpoint response by assessing phosphorylated SUN-1^{S8} staining, which revealed prompt activation of the checkpoint, manifested by the extended loading of pSUN-1^{S8} at the nuclear envelope as early as 5 h of exposure to auxin (Figures 2C and S2D). After 24 h of exposure to auxin, a further robust prolongation of pSUN-1^{S8} loading was observed, as was similarly found in the spo-11(ok79) null allele (Woglar et al., 2013), indicating that impaired RAD-51 loading stemming from abolished DSBs in the spo-11::AID::3xFLAG worms exposed to auxin at 5 h is already sufficient to elicit checkpoint activation in mid-late pachytene cells. Importantly, the comparable phospho-SUN-1^{S8} prolongation in the worms exposed to auxin was age-independent indicating, once more, that exposure to auxin in L4s or young adults elicits the same effects.









Preventing SPO-11 function at later stages abrogates chiasmata formation

Next, we sought to investigate how modulating SPO-11 levels would influence CO establishment. Establishment of chiasmata is a multi-step process that proceeds through spatiotemporally separated events in the gonad. In fact, upon completion of RAD-51-mediated strand invasion by early to mid-pachytene transition, early pro-CO factors RMH-1 and MSH-5 display loading at presumably all recombination intermediates, followed by reinforcement and designation of putative CO sites, which then become proficient in COSA-1 loading at late pachytene stage (Jagut et al., 2016; Yokoo et al., 2012). The cytological manifesta-

Figure 2. SPO-11 mediates DSB induction at different stages of meiotic prophase I

(A) Quantification of BAD-51 foci across the gonad at different exposure times to auxin. The x axis indicates the zones along the gonad and the y axis the average number of foci in each zone. PMT, premeiotic tip; TZ, transition zone; EP, early pachytene; MP, mid-pachytene; LP, late pachytene. Asterisks indicate statistical significance calculated by Mann-Whitney test (***p < 0.0001; NS, not significant). Data are represented as mean \pm SEM. (B) Quantification of RAD-51 foci upon auxin exposure followed by recovery on plates devoid of auxin, performed as in (A). Asterisks indicate statistical significance calculated by Mann-Whitney test (***p < 0.0001; **p = 0.0001; NS, not significant). Data are represented as mean \pm SEM. (C) Quantification of pSUN-1S8-positive cells in worms of the indicated age exposed to auxin for the indicated times. Data are represented as mean ± SD and asterisks indicate statistical significance calculated by χ^2 test (p < 0.1). At least three gonads for each time point were used for quantifications

tion of a CO occurrence (chiasma), however, is not visible until diakinesis stage. where it holds each pair of bivalents together with cohesins. Nuclei in late pachytene take several hours to reach diakinesis stage (roughly 12 h, but likely closer to 20-22 h), as corroborated by the fact that full rescue of bivalent formation in irradiated spo-11 nulls does not occur until about 24 h have elapsed from the time of irradiation (Dernburg et al., 1998; Janisiw et al., 2020; Yokoo et al., 2012). For this reason, monitoring the effects of SPO-11 depletion on the formation (or abrogation) of CO-designation sites in late pachytene cells and how these translate into establishment (or lack) of chiasmata in diakinesis nuclei requires a different temporal assessment in the two gonad compartments (Figure 3).

We exposed OLLAS::cosa-1; spo-11:: AID::3xFLAG worms at different time win-

dows and analyzed both establishment of CO-designation sites in late pachytene nuclei by monitoring COSA-1 recruitment to chromatin foci, as well as DAPI bodies in diakinesis nuclei. Our analysis revealed almost complete lack of CO sites when nuclei are depleted in a time window corresponding to mid to late pachytene (Figure 3). Nuclei that were only depleted earlier in meiosis (24-h depletion + 24-h recovery for COSA-1, 24-h depletion + 48-h recovery for diakinesis) did not show loss of chiasmata. Most importantly, depletion for a short time window of 12 h (1.5 zones) was sufficient to elicit significant loss of chiasmata, as long as that corresponded to mid to late pachytene (12-h depletion + 6-h recovery for COSA-1, 12-h depletion +

Article



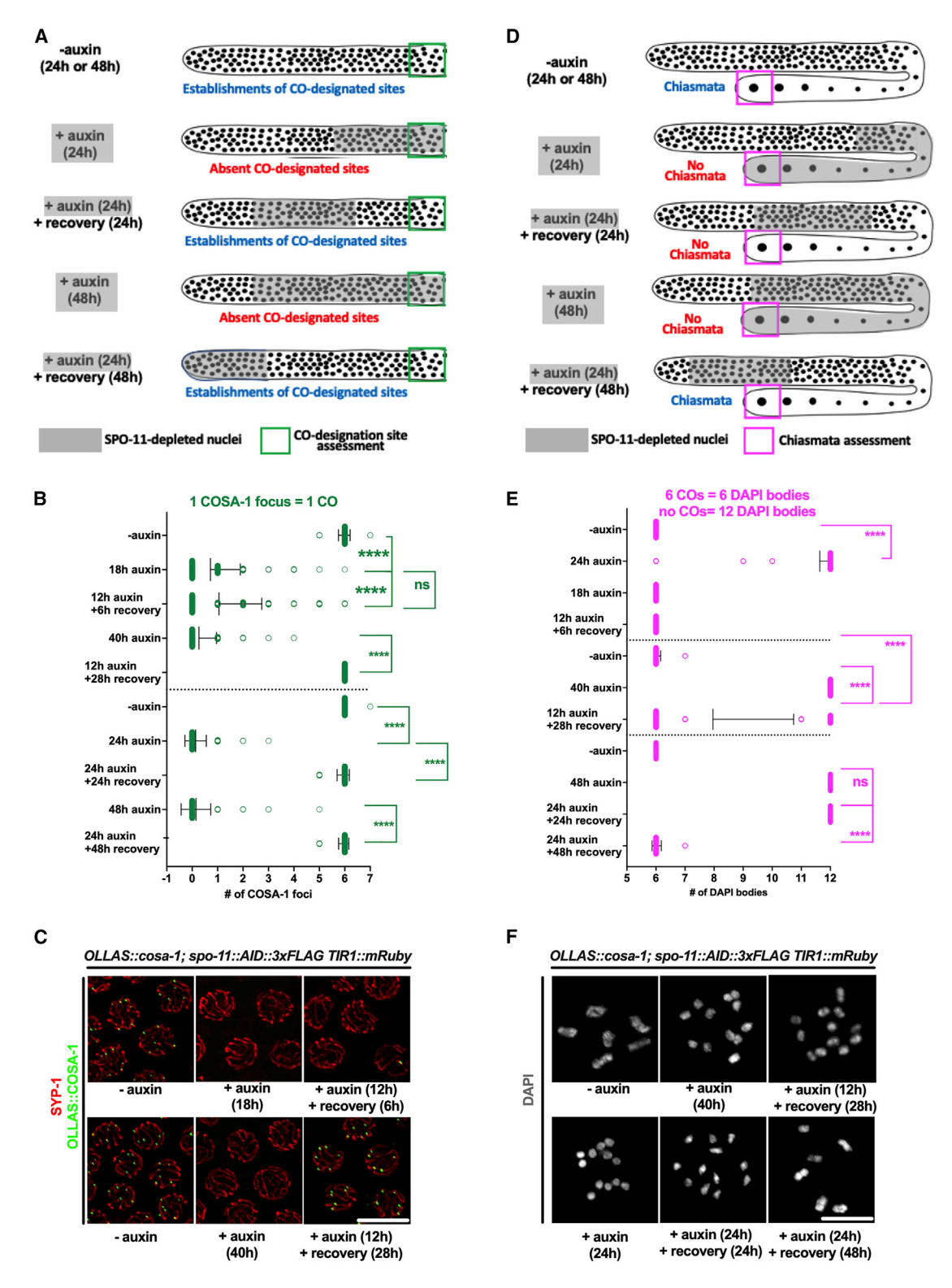


Figure 3. Preventing SPO-11 function in later stages abrogates chiasmata formation

(A) Schematic representation of the experimental setting employed for assessment of COSA-1. Gray areas indicate area of the gonad undergoing SPO-11 depletion at the indicated times.

(B) Quantification of COSA-1 foci at the indicated time points and conditions (auxin, non-auxin, or upon recovery on non-auxin plates). Asterisks indicate statistical significance as assessed by t test (****p < 0.0001; NS, not significant).

(legend continued on next page)



28-h recovery for diakinesis). Induction of exogenous DSBs by ionizing radiation triggered a robust rescue in chiasmata formation on worms grown on auxin plates for 48 h without recovery (Figure S3B), confirming that absence of bivalents is due to a lack of DSBs. These results further reinforce that formation of SPO-11-dependent breaks occurs both at meiosis onset and mid-late pachytene stage, and that, strikingly, DSBs generated during mid-late pachytene stage are essential to yield COs. As for DAPI body analysis, we confirmed that exposure to auxin was not perturbing bivalent formation (Figure S2E).

To complement this analysis, we also monitored loading of HA:RMH-1 (Janisiw et al., 2018, 2020) after 16-h exposure to auxin, which revealed a severe impairment throughout the germline and was largely, although not completely, restored after 28 h of recovery (Figure 4A). This indicates that CO-designation sites arising upon rescued DSB-dependent formation of recombination intermediates were established in both mid and late pachytene and thus that SPO-11-mediated cleavage occurs at both early and at later stages. Importantly, RMH-1 loading (which, unlike COSA-1's, is triggered also at earlier stages during meiotic progression; Jagut et al., 2016) was selectively recovered in mid to late pachytene cells but not earlier on, as similarly observed for RAD-51 (Figure 2B).

Absence of recombination intermediates arising from a lack of DSBs prevents inter-homolog recombination and therefore CO formation. It has been previously shown that establishment of COs triggers chromosome remodeling, a process whereby the central elements of the synaptonemal complex are retained on the short arm of the bivalent (harboring the CO site), whereas axes components define both the long and the short arm (i.e., HTP-3 and HIM-3) (Couteau et al., 2004; Goodyer et al., 2008) or are only confined along the long arm (HTP-1/2) (Martinez-Perez et al., 2008). If COs fail to form, both central and lateral elements display an overlapping localization. Given the impaired loading of RAD-51 and pro-CO factors, we wanted to assess whether bivalent remodeling also failed to take place by analyzing SYP-1 and HTP-1 staining. As shown in Figure 4B, unlike in the controls, SYP-1 retraction to the short arm of the bivalent did not occur in late pachytene and diplotene nuclei in spo-11::AID::3xFLAG worms exposed to auxin, in which an extensive co-localization with HTP-1 was instead observed. This further corroborates that, in the nuclei where depletion of SPO-11 occurred at mid-pachytene stage, recombination intermediates are not formed and consequentially CO formation is abrogated.

EXO-1/DNA-2 act redundantly in LRR

Next, we tested whether early and late breaks also associate with distinct modes of DSB processing. While the role of EXO-1 in LRR was previously examined via its effect on RAD-51 localization (Lemmens et al., 2013; Yin and Smolikove, 2013), DNA-2's was not. DNA-2 is essential for mitotic replication, so its knockout confers a complex phenotype due to an accumulation of DNA damage in pre-meiotic germline nuclei (Lee et al., 2003). To assess the role of LRR, we performed auxin-mediated degradation of DNA-2 (Figures S4 and S5A), by itself or in combination with knockout of exo-1 (Figures 5, 6A, S4B, S4C, and S5A). While removal of exo-1 leads to accumulation of RAD-51 foci as previously reported (Lemmens et al., 2013; Yin and Smolikove, 2013), depletion of DNA-2 reduced both the number and intensity of RAD-51 foci, and double mutants confer a stronger effect both on RAD-51 foci numbers and intensity (Figures 5A-5C). These data are consistent with both DNA-2 and EXO-1 acting in LRR, with DNA-2 playing a more important role. Most importantly, we found that 4-h depletion is sufficient to inhibit RAD-51 focus formation in zone 6 of LRR mutant germlines (Figures 5A, S4C, and S5C). Taking into account the rate of nuclear movement in the germline, most DSBs that were impaired in resection originated in the same zone in which they were processed, suggesting that meiotic resection is a rapid process. The strong effect that is seen with only 4-h depletion of DNA-2 at the late pachytene transition agrees with the findings from our SPO-11 depletion experiments, indicating that DSBs are formed at later than previously speculated stages of meiosis.

EXO-1 and DNA-2 act predominantly on late meiotic **DSBs**

Unlike what we observed for SPO-11 depletion, removing DNA-2 and EXO-1 does not bear the same magnitude of effect throughout prophase I; we observed a stronger effect on midlate pachytene (zone 6, 89% depletion and zone 7, 97% depletion of RAD-51 foci) than mid-pachytene (zone 5, 39% depletion of RAD-51 foci; Figure 5A) DSBs (Figures 5A and S5A). The attenuated effect on early DSBs did not change with longer exposures (Figures 6A and S5A), indicating that it is not influenced by changes in DSB turnover. Moreover, if the persistence of DSBs in zone 5 was due to delayed repair (RAD-51 foci persistence), foci would remain in similar intensity. However, we observed that foci in zone 5 become dimmer after EXO-1 and DNA-2 depletion (~40% intensity of wild type; Figure 5C). Thus, the differences between zone 5 and 6 likely reflect reduced dependence on EXO-1 and DNA-2 in zone

The reduced dependence on EXO-1 and DNA-2 in prophase may be reflected in the levels of their nuclear localization. Indeed, while DNA-2 and EXO-1 did show localization to all germline nuclei, the pattern changed throughout prophase in a specific manner for these nucleases (Figures 6B-6E); DNA-2 was enriched at PMT and LP, while EXO-1 showed higher expression in the distal germline. DNA-2 and EXO-1 localized throughout the nucleus and did not form discrete foci corresponding to the expected number of DSBs by RAD-51 focus analysis. This property is shared with many other repair factors, including

⁽C) Representative images of nuclei analyzed for quantifications. Scale bar, 5 µm.

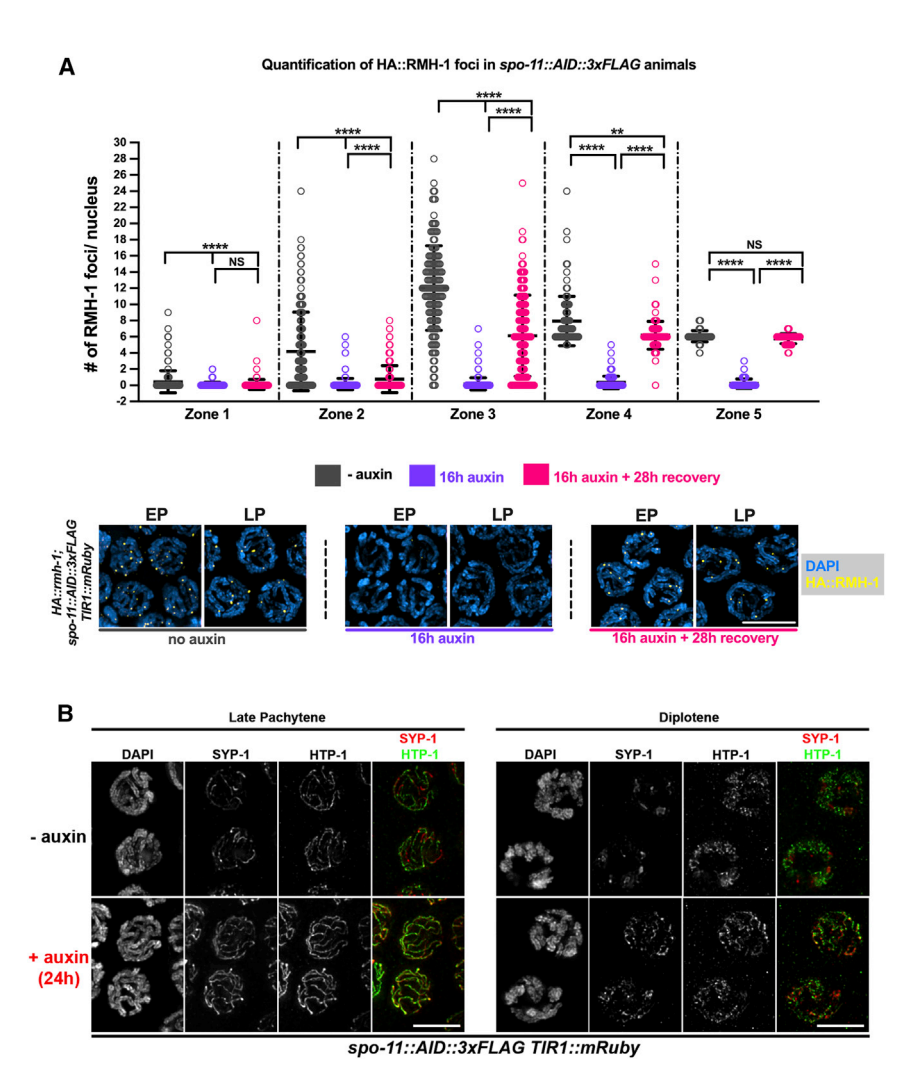
⁽D) Schematic representation of the experimental setting employed for assessment of chiasmata.

⁽E) Quantification of DAPI bodies at the indicated time points and conditions (auxin, non-auxin or upon recovery on non-auxin plates). Asterisks indicate statistical significance as assessed by t test (****p < 0.0001; NS, not significant).

⁽F) Representative images of nuclei analyzed for quantifications. Scale bar, 5 μm. All analyses were performed in biological duplicates.

Article





MRE-11 (Harrell et al., 2021; Reichman et al., 2018), indicating that the DSB-localized fraction is small compared with the total. Nuclear localization levels of each of these nucleases were only mildly affected by the absence of the other, indicating that they likely act independently (Figures S5B-S5E). To examine whether EXO-1 and DNA-2 localize to DSBs, we exposed the germline to laser microirradiation (Harrell et al., 2018) (Figure 6F, 6G, and S5I). Consistently, despite low levels of DNA-2 expression in late pachytene, DNA-2 was recruited to DNA damage efficiently (and comparably with pre-meiotic nuclei), whereas its recruitment was impaired in early pachytene (Figures 6F and S5I). Consistent with a minor role for EXO-1 in LRR, both EXO-1 expression level and its localization to DNA damage were not increased in later meiotic stages (Figures 6G and S5F). These data suggest that zone 5 and 6 likely reflect reduced activity of EXO-1 and DNA-2, compensated for by an alternative, yet unidentified, LRR resection pathway capable of generating limited length of resection tracts (dimmer foci).

Last, we wanted to exclude that the differences observed in RAD-51 foci numbers through the germline are due to variable auxin-mediated degradation. Our experiments were done in

Figure 4. Analysis of HA::RMH-1 and chromosome remodeling upon SPO-11 deple-

(A) Quantification of HA::RMH-1 foci and representative images of nuclei at the indicated stages, under the specified conditions. Gonads were divided into five equal regions from transition zone to pachytene exit. Asterisks indicate statistical significance calculated by Mann-Whitney test (****p < 0.0001; NS, not significant). Data are represented as mean + SD.

(B) Representative images of nuclei at the indicated stages and conditions, stained for SYP-1/ HTP-1. Scale bar, 5 μm. All analyses were performed in biological duplicates.

the null exo-1 background, excluding that the differences are due to differential expression of EXO-1. To test whether auxin-mediated degradation of DNA-2 was less efficient in zone 5 compared with zone 6, we measured nuclear intensity of DNA-2 before and after auxin exposure. DNA-2 levels were above background in both zones 5 and 6 without auxin and 30 min post exposure, but fell to background levels at later time points (Figures 6H, S5G, and S5H). Importantly, DNA-2 levels were equal or lower in zone 5 compared with zone 6 throughout the experiment, indicating that the attenuated resection in zone 5 is not due to delayed degradation of DNA-2. Altogether, this suggests that EXO-1 and DNA-2 play a more dominant role in late-DSB processing and early LRR can be mediated by an EXO-1 and DNA-2-indepen-

dent mechanism that produces shorter resection tracts (see section "discussion").

LRR is required but not essential for CO formation and inhibition of cNHEJ

Abrogating LRR had a profound effect on DSB processing; however, based on RAD-51 foci number counts, about one-third of DSBs were still resected (Figures 5A-5C). Based on estimated levels of DSBs in wild type (Gao et al., 2015; Rosu et al., 2011), these likely translate to about three DSBs per chromosome that are resected to provide enough ssDNA for RAD-51 loading to form a visible focus. Irradiation experiments have demonstrated that similar levels of DSBs are sufficient to form an obligatory CO (Yokoo et al., 2012). We hypothesized that DSB resection is impaired but not abolished in LRR mutants; thus, chiasma formation would still occur, even in oocytes from nuclei depleted for LRR. Indeed, depleting LRR in mid- to late pachytene did not lead to complete disruption of chiasmata, although 30%-39% of the oocytes depleted of LRR in pachytene showed at least one abnormal DAPI body (Figures 7A and 7B). Depletion of LRR in early pachytene led to smaller effects compared with



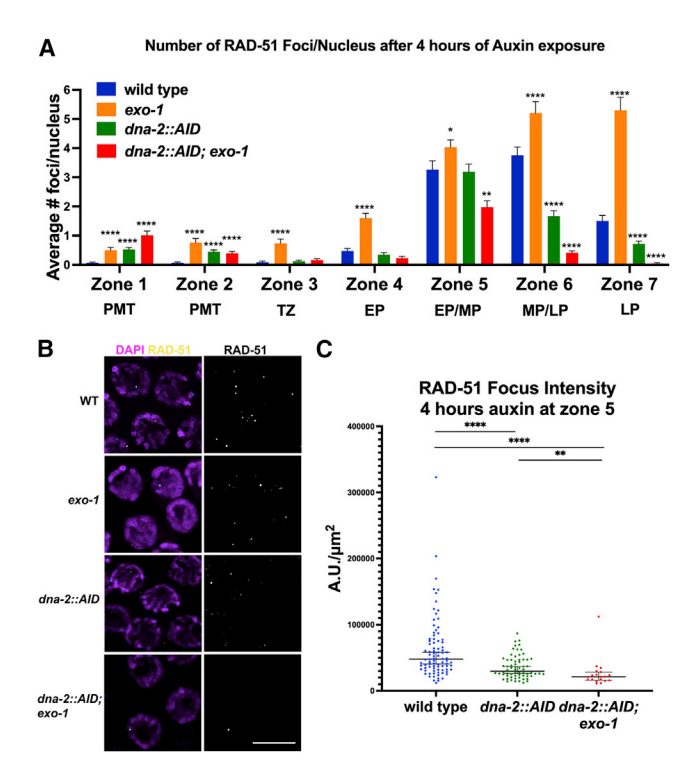


Figure 5. LRR is required for resection in late meiotic prophase I

(A) Quantification of RAD-51 foci across the gonad in the indicated genotypes. The x axis indicates the zones along the gonad and the y axis the average number of foci in each zone. Asterisks indicate statistical significance calculated by Mann-Whitney test (****p < 0.0001,***p < 0.001,**p < 0.01, and *p < 0.05) and reflect statistical comparison with wild type.

- (B) Representative images from zone 6. Scale bar, 5 μm.
- (C) Quantification of RAD-51 focus intensity in the indicated genotypes (exposure as in A). Each data point is a nucleus. Asterisks indicate statistical significance calculated by Mann-Whitney test (****p < 0.0001,***p < 0.001,**p < 0.01, and *p < 0.05). All analyses were performed in at least three gonads and in biological replicates.

mid- to late pachytene depletion, which is consistent with a more dominant role for LRR in mid-late pachytene.

Abnormal DAPI bodies can be indicative of fusion events, univalents, or fragmentation. While fusions lead to decreased DAPI body counts, the latter two result in an increase in DAPI body counts. To identify which mechanisms are responsible for the abnormal DAPI bodies, we combined LRR mutants with mutants that abrogate COs or cNHEJ (Figures 7C-7F). Formation of bivalents was dependent on MSH-5 (with no further increase in DAPI bodies numbers above the expected 12 univalents) (Figures 7C, 7D, and S6A), while formation of DAPI bodies indicative of chromosomal fusions was dependent on cKU-70 (Figures 7E and 7F). In agreement, cKU-80 levels slightly increased following auxin exposure in most germline regions, while it has no effect on wild-type cells (Figures 7G, 7H, and S6B). These data altogether indicate that LRR-impaired mutants can support CO formation, but a small fraction of DSBs that do not form COs are either not engaged in any repair pathways (univalent) or are targeted to repair by cNHEJ (chromosomal fusions).

DISCUSSION

Studies in many organisms show that recombination intermediates (Dmc1/Rad51) persist through the pachytene stage (Bishop, 1994; Dernburg et al., 1998; Enguita-Marruedo et al., 2019). In C. elegans, evidence for an extended DSB formation window was attributed to localization of DSB licensing factors (DSB-1/ 2/3) (Hinman et al., 2021; Rosu et al., 2013; Stamper et al., 2013). However, this localization was not abolished in SPO-11 mutants, indicating that it is not a direct indication of DSB formation activity (Rosu et al., 2013; Stamper et al., 2013). Here we have shown that RAD-51 foci turn over rapidly (less than 4 h) from meiotic entry to mid- to late pachytene transition, providing direct evidence for continuous DSB formation. These findings also extend the proposed window of meiotic DSB formation in C. elegans from ending in early pachytene to the late pachytene transition, where the last SPO-11-induced DSBs are observed.

SPO-11-dependent DSBs are repaired as CO or NCOs. Early studies using excision of transposable elements indicated that CO and NCOs can both be generated in any stage of meiotic prophase I (Rosu et al., 2011). However, breaks induced by such an excision event are very different from SPO-11-induced breaks (do not involve covalent binding of a protein to a break that is coupled to resection; Richardson et al., 2006; Robert et al., 2008). Our findings challenge the notion that meiotic DSBs have similar fates; we found that late DSBs are required for CO formation, while early DSBs are not. We suggest that the extension of the DSB proficient window serves a role in promoting CO formation. A related phenomenon may be "scout DSBs" identified in yeast, which are somewhat analogous to early DSBs (Joshi et al., 2015; Sandhu et al., 2020). Scout DSBs are DSBs formed at meiotic entry, before homolog engagement, and thus are repaired from the sister chromatid and not the homolog as later DSBs are. However, one big difference is that yeast scout DSBs are formed prior to homolog engagement, thus these early DSBs cannot choose the homolog as a template for repair, while most C. elegans early DSBs are formed in a germline region where the synaptonemal complex is fully assembled and there is no block of repair from the homologous chromosomes. The mechanism channeling early DSBs to NCO and late DSBS to CO is unknown.

Mutants in genes encoding for HR proteins activated a checkpoint leading to ~50% extension of DSB-1/2/3 and pSUN-1 window (Rosu et al., 2013; Woglar et al., 2013). A similar effect is seen in our SPO-11 depletion. This checkpoint is believed to increase DSB formation to attempt mitigation of the recombination defects. Indeed, up to 2 h following SPO-11 depletion, but not later, RAD-51 foci persist in mid- to late pachytene, consistent with upregulation of SPO-11 activity. It is possible that such an effect is achieved in the short time frame in which SPO-11 levels drop but are not fully eliminated. It is important to note that these additional DSBs are formed on top of the natural DSBs (non-checkpoint activated DSBs) that are present in late pachytene, and these DSBs also disappear in the 4-h window. Thus, all forms of SPO-11-induced RAD-51 foci turn over in less than 4 h.

When DSB repair is proficient, RAD-51-ssDNA filaments persist until strand invasion (Carver and Zhang, 2021). Then

Article



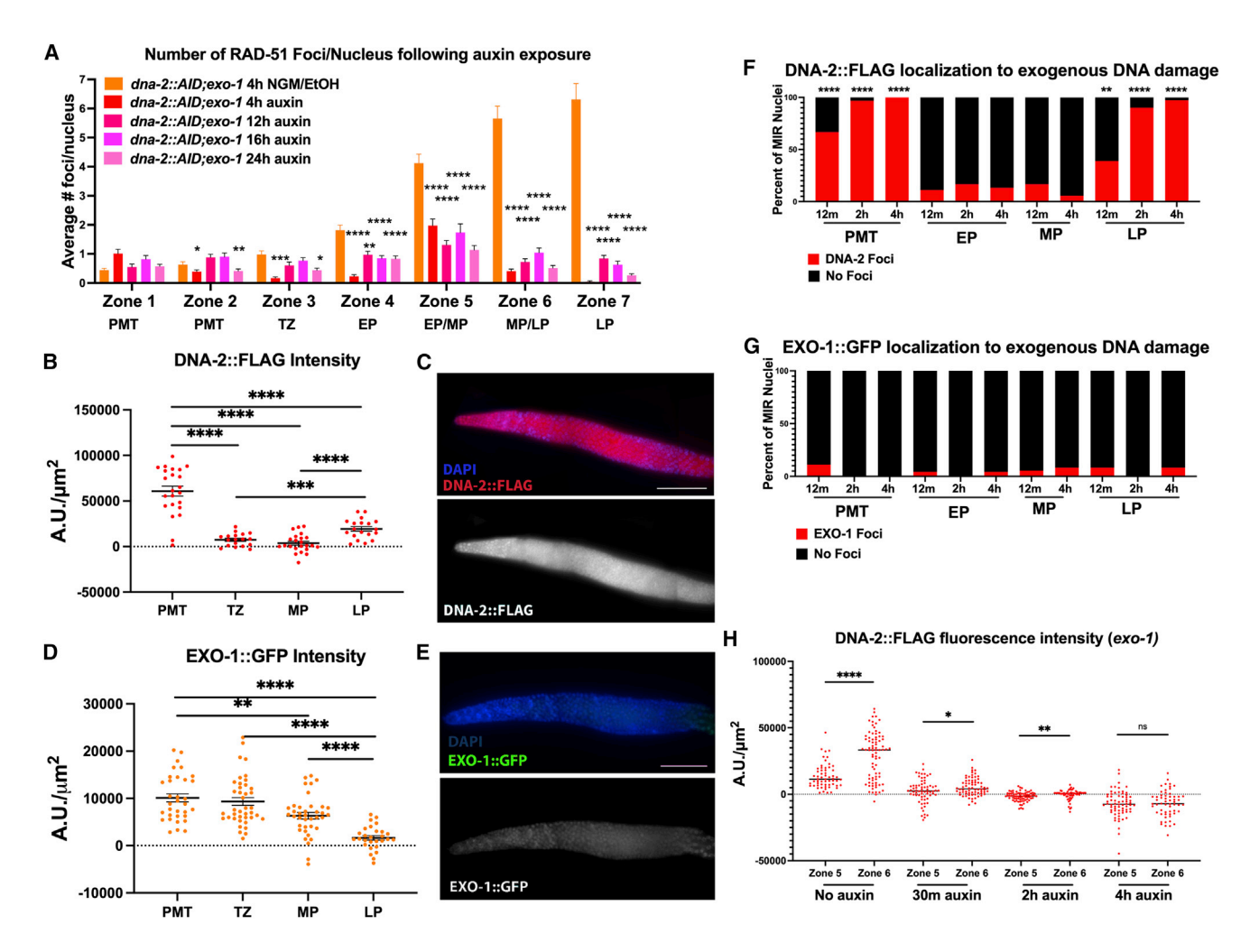


Figure 6. Impaired LRR leads to formation of univalents and cNHEJ-mediated chromosomal fusions

(A) Quantification of RAD-51 foci across the gonad of dna-2::AID; exo-1 mutants at different exposure times in 1-day-old adults to auxin (red and pink bars) or without (orange bar). The x axis indicates the zones along the gonad and the y axis the average number of foci in each zone. DNA-2 depleted in 4 h auxin, mostly in the same zone it is counted at; 12 h auxin, in the same zone it is counted at and a zone before; 16 h auxin, in the same zone it is counted at and 1.5 zones before; 24 h auxin, in the same zone it is counted at and two zones before. Statistical analysis comparing with EtOH.

- (B) Quantification of DNA-2 nuclear intensity (y axis) in the indicated genotypes throughout the germline. Each data point is a nucleus.
- (C) Representative images of germline localization of DNA-2 under wild-type conditions. Scale bar, 40 µm.
- (D) Quantification of EXO-1 nuclear intensity (y axis) in the indicated genotypes throughout the germline.
- (E) Representative images of germline localization of EXO-1 (bottom) under wild-type conditions. Scale bar, 40 μm.

(F and G) Microirradiation-targeted nuclei with the indicated recovery times (x axis). The y axis indicates the percentage of targeted nuclei with (red) or without (black) foci for DNA-2::FLAG (F) or EXO-1::GFP (G).

(H) DNA-2:FLAG in zone 5 and zone 6 (EP/MP and MP/LP, respectively) nuclei with the indicated exposure times to auxin (x axis). (A, B, D, and F-H) Asterisks indicate statistical significance calculated by Mann-Whitney test (A, B, D) or Fisher's exact test (F-H): **** p < 0.0001, ***p < 0.001, ***p < 0.01, and *p < 0.05. Data are represented as mean \pm SEM. All analyses were performed in at least three gonads and in biological replicates.

RAD-51 is removed by proteins such as RAD-54, which enables DNA synthesis, an obligatory step in any HR pathway. Thus, the time it takes for the RAD-51 foci to disappear in our SPO-11 depletion experiments reflects the maximal time from DSB formation to strand invasion (minus the 30-60 min to degrade proteins using the AID system we use in our studies; Ashley et al., 2021; Zhang et al., 2015). Our results are consistent with a quick turnover of DSBs from the point of SPO-11 cutting to strand invasion, suggesting that resection of meiotic DSBs occurs in less than 3.5 h. Quick turnover is consistent with resection of other forms of DNA damage (Hayashi et al., 2007; Koury et al.,

Studies in yeast cells and in human germline cells suggest that DSB formation and pre-meiotic replication are connected events. In yeast, replication inhibition activates a checkpoint that prevents DSB formation, and DSB-associated proteins and replication origins locally compete on Cdc28(CDK-S) and Cdc7 (Murakami and Keeney, 2008). In mice and humans, there is a significant overlap between origins of replication and DSB sites, suggesting that DSBs are established during replication



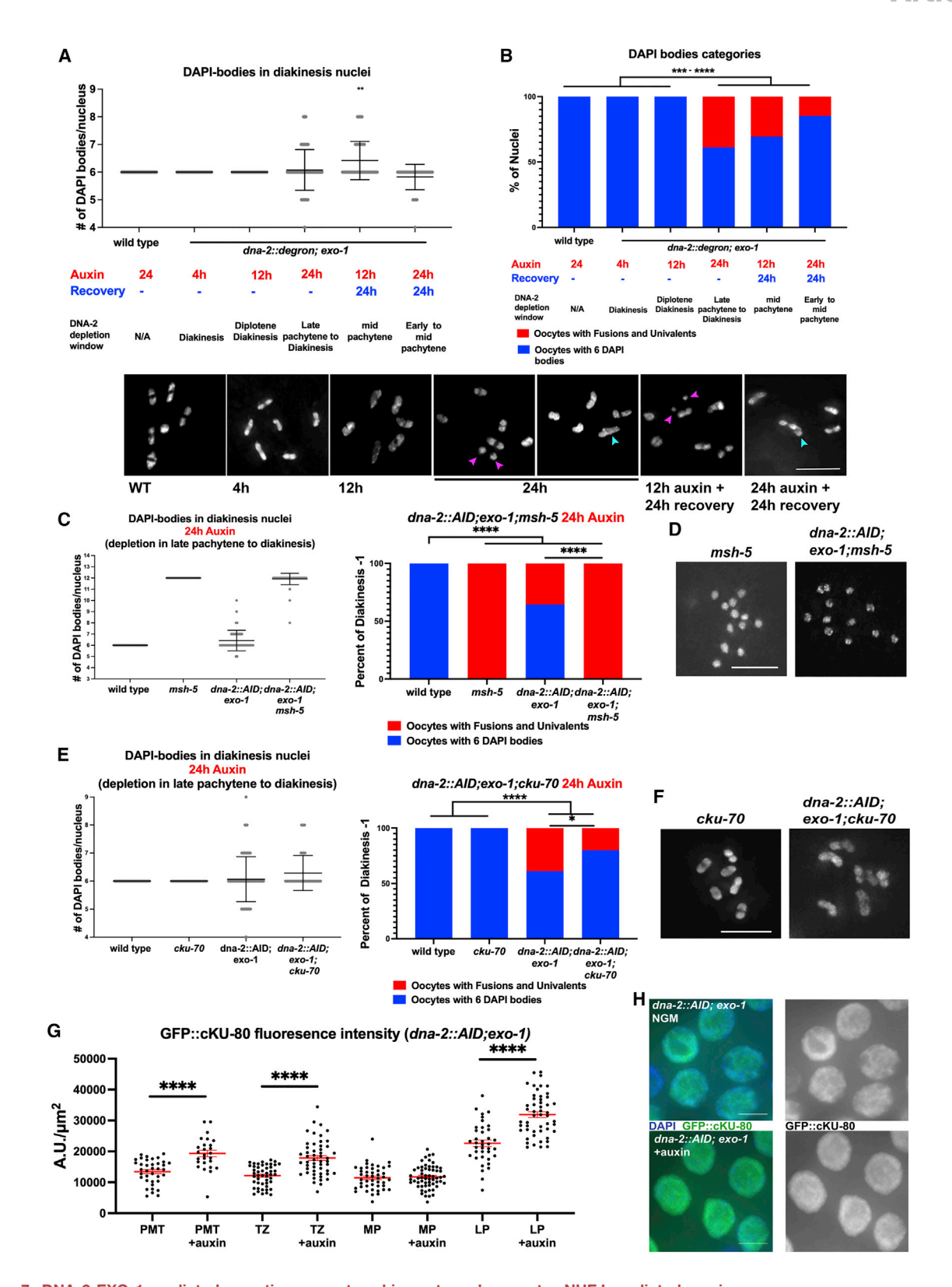


Figure 7. DNA-2-EXO-1-mediated resection promotes chiasmata and prevents cNHEJ-mediated repair (A) Quantification of DAPI bodies in diakinesis nuclei upon auxin exposure at the indicated times. Left: each data point is a diakinesis -1 oocyte. (B) The same data divided into two categories as indicated. Representative images at bottom. Pink arrow heads, univalent; blue arrow heads, fusions. Scale bar, 5 μm.

Article



(Pratto et al., 2021). We show that, following recovery from SPO-11 depletion, early DSBs, unlike late DSBs, can be established only in cells that passed through pre-meiotic replication. These data suggest a conserved connection between passage through replication and DSB formation licensing. This licensing may be done through interactions with origins of replication or through interaction with the meiotic axis, such as through HTP-3. HTP-3 assembles on chromosomes in PMT, and is required for DSB formation (Goodyer et al., 2008). The observed phenotypes can also be due to differential regulation of spo-11, taking longer to transcribe or translate SPO-11 in the early DSB region.

In somatic cells, both EXO1- and DNA-2/BLM are required for resection (Cejka, 2015). During meiosis, both of these nucleases play a role. However, while EXO-1 plays a major role in yeast, in mice, exo-1 mutants show mild resection defects (Garcia et al., 2011; Paiano et al., 2020; Yamada et al., 2020; Zakharyevich et al., 2010). In our studies, we show that EXO-1 plays a role in resection, as suggested in other studies, but DNA-2's role is more central. Thus, in metazoans, the roles of these two resection pathways are flipped, with DNA-2 taking the lead role. Despite the importance of EXO-1 and DNA-2/BLM to resection and preventing aberrant repair, resection is not completely inhibited, and shorter resection tracts can support CO formation in most cells.

Our studies also provide an intriguing observation: in midpachytene, a DNA-2/EXO-1-independent pathway ensues. This pathway can generate ssDNA that loads RAD-51, but likely forms shorter resection tracts than EXO-1/DNA-2 LRR (dim RAD-51 foci). This EXO-1/DNA-2-independent LRR pathway may involve an as-yet unidentified nuclease, or it can involve a modified activity of a known nuclease: MRE-11. Resection tracts in meiosis are at the 1- to 2-kb range. Given RAD-51 focus intensity in the dna-2; exo-1 depletion conditions is ~40% of wild-type, we speculate that the modified LRR mechanism can resect DSBs to a 0.4- to 0.8-kb length. This is close to the range of some Mre11 cut sites in yeast meiosis (0.3 kb away from Spo11; Garcia et al., 2011).

To conclude, we found that meiotic DSBs occur throughout most of meiotic prophase and turn over quickly. Moreover, DSBs are not homogeneous: early and late DSBs are distinct in terms of both their processing and their fated repair outcome. Although it is tempting to connect these two observations, our data do not directly provide a clear relationship. Our studies do, however, reveal that the context of DSB formation plays a pivotal role in the repair and sets the stage for future identification of these regulatory mechanisms.

Limitations of the study

The limitations of these study are the following: (1) due to different reagents employed for RAD-51 detection, the observed kinetics are not identical between experiments (as found in other studies in the field) and should be compared only within a specific experimental setting with its internal controls; (2) the inability to detect SPO-11 can result in over-estimation of the time required for DSB turnover; therefore, the actual time from DSB formation to strand invasion may be shorter than our estimation of 4 h. Moreover, the inability to detect SPO-11 prevents us from testing alternative hypotheses to explain why SPO-11 recovery is inhibited in early versus late prophase (differential expression, degradation, or maturation of SPO-11); (3) minor effects in the rate of nuclear movement may not be detected by the EdU assay, which may lead to small adjustment of the time windows of NCO versus CO targeted breaks; (4) activation of pSUN-1^{S8} checkpoint can have unexpected effects, such as mis-regulating repair pathway choice; (5) although our results are consistent with limited effects of differential degradation of DNA-2 along the gonad, we cannot rule out that other processes may affect DNA-2 activity differently in the germline.

STAR*METHODS

Detailed methods are provided in the online version of this paper and include the following:

- KEY RESOURCES TABLE
- RESOURCE AVAILABILITY
 - Lead contact
 - Materials availability
 - Data and code availability
- EXPERIMENTAL MODEL AND SUBJECT DETAILS
 - Worm lines
 - Bacterial strains
 - Rats
- METHOD DETAILS
 - *C. elegans* genetics
 - Auxin treatment
 - Generation of SYP-1 antibody
 - Antibody staining
 - Image acquisition
 - Ethanol fixation
 - Western blot
 - UV laser microirradiation
 - Fluorescence intensity
 - Meiotic progression with EdU
 - O CRISPR/Cas9 genome editing
- QUANTIFICATION AND STATISTICAL ANALYSIS

⁽C) Quantification of DAPI bodies in diakinesis nuclei upon 24-h auxin exposure in the indicated genotypes. Left: each data point is a diakinesis - 1 oocyte. Right: the same data divided into two categories as indicated.

⁽D) Representative images of diakinesis -1 oocytes in (C). Scale bar, 5 μm .

⁽E) Quantification of DAPI bodies in diakinesis nuclei upon 24-h auxin exposure in the indicated genotypes. Left: each data point is a diakinesis -1 oocyte. Right: the same data divided into two categories as indicated.

⁽F) Representative images of diakinesis -1 oocytes in (C). Scale bar, 5 μm.

⁽G) Fluorescence intensity measurements of GFP::cKU-80 in dna-2::AID; exo-1 germlines. Each data point reflects a measurement in one nucleus.

⁽H) Representative image of late pachytene nuclei from (G). Scale bar, 4 µm. (A-C) Asterisks indicate statistical significance calculated by Mann-Whitney test (left) or Fisher's exact test (right): ****p < 0.0001, ***p < 0.001, ***p < 0.001, and *p < 0.05. Data are represented as mean \pm SEM. Analyses were repeated at least twice and in biological replicates.





SUPPLEMENTAL INFORMATION

Supplemental information can be found online at https://doi.org/10.1016/j. celrep.2022.111403.

ACKNOWLEDGMENTS

We are grateful to E. Martinez-Perez, V. Jantsch, and D. Libuda for the anti HTP-1, anti phospho-SUN-1^{S8} and GFP::cku-80 strain, and anti RAD-51 (used for the analysis in Figure 2) antibodies respectively; and to Lumír Krejči, David Šmajs, and Stjepan Uldrijan for sharing equipment. We thank Dylan Cooke and Kailey Harrell for their help with generating the exo-1::flag::GFP strain and Emily Koury for her help with dna-2::degron::3xFLAG. We acknowledge the core facility CELLIM supported by the Czech-Biolmaging large RI project (LM2018129 funded by MEYS CR) for their support with obtaining scientific data presented in this paper. Research in the Silva lab is funded by the Czech Science Foundation (GAČR, GA20-08819S) and a Start-up grant from the Department of Biology, Faculty of Medicine, of Masaryk University. Research in the Smolikove lab is funded by the National Science Foundation (NSF 2027955).

AUTHOR CONTRIBUTIONS

T.H., M.E., R.B., S.T., H.T., A.D., C.C., S.S., and N.S. performed the experiments. T.H., S.S., and N.S. designed the research. S.S. and N.S. acquired funding. S.S., T.H., and N.S. wrote the manuscript.

DECLARATION OF INTERESTS

The authors declare no competing interests.

Received: January 10, 2022 Revised: June 1, 2022 Accepted: September 1, 2022 Published: September 27, 2022

REFERENCES

Almanzar, D.E., Hamrick, A., and Rog, O. (2022). Single-sister labeling in the C. elegans germline using the nucleotide analog EdU. STAR Protoc. 3, 101344. https://doi.org/10.1016/j.xpro.2022.101344.

Ashley, G.E., Duong, T., Levenson, M.T., Martinez, M.A.Q., Johnson, L.C., Hibshman, J.D., Saeger, H.N., Palmisano, N.J., Doonan, R., Martinez-Mendez, R., et al. (2021). An expanded auxin-inducible degron toolkit for Caenorhabditis elegans. Genetics 217, iyab006. https://doi.org/10.1093/genetics/iyab006. Bishop, D.K. (1994). RecA homologs Dmc1 and Rad51 interact to form multiple nuclear complexes prior to meiotic chromosome synapsis. Cell 79, 1081-1092. https://doi.org/10.1016/0092-8674(94)90038-8.

Borde, V. (2007). The multiple roles of the Mre11 complex for meiotic recombination. Chromosome Res. 15, 551-563. https://doi.org/10.1007/s10577-007-1147-9.

Brenner, S. (1974). The genetics of Caenorhabditis elegans. Genetics 77,

Carver, A., and Zhang, X. (2021). Rad51 filament dynamics and its antagonistic modulators. Semin. Cell Dev. Biol. 113, 3-13. https://doi.org/10.1016/j. semcdb.2020.06.012.

Cejka, P. (2015). DNA end resection: nucleases team up with the right partners to initiate homologous recombination. J. Biol. Chem. 290, 22931-22938. https://doi.org/10.1074/jbc.R115.675942.

Chin, G.M., and Villeneuve, A.M. (2001). C. elegans mre-11 is required for meiotic recombination and DNA repair but is dispensable for the meiotic G2 DNA damage checkpoint. Genes Dev. 15, 522-534. https://doi.org/10.1101/ gad.864101.

Choi, K., Zhao, X., Tock, A.J., Lambing, C., Underwood, C.J., Hardcastle, T.J., Serra, H., Kim, J., Cho, H.S., Kim, J., et al. (2018). Nucleosomes and DNA methylation shape meiotic DSB frequency in Arabidopsis thaliana transposons and gene regulatory regions. Genome Res. 28, 532-546. https://doi.org/10. 1101/gr.225599.117.

Couteau, F., Nabeshima, K., Villeneuve, A., and Zetka, M. (2004). A component of C. elegans meiotic chromosome axes at the interface of homolog alignment. synapsis, nuclear reorganization, and recombination. Curr. Biol. 14, 585-592. https://doi.org/10.1016/j.cub.2004.03.033.

Dernburg, A.F., McDonald, K., Moulder, G., Barstead, R., Dresser, M., and Villeneuve, A.M. (1998). Meiotic recombination in C. elegans initiates by a conserved mechanism and is dispensable for homologous chromosome synapsis. Cell 94, 387-398. https://doi.org/10.1016/S0092-8674(00)81481-6.

Enguita-Marruedo, A., Martín-Ruiz, M., García, E., Gil-Fernández, A., Parra, M.T., Viera, A., Rufas, J.S., and Page, J. (2019). Transition from a meiotic to a somatic-like DNA damage response during the pachytene stage in mouse meiosis. PLoS Genet. 15, e1007439. https://doi.org/10.1371/journal.pgen. 1007439

Gao, J., Kim, H.-M., Elia, A.E., Elledge, S.J., and Colaiácovo, M.P. (2015). NatB domain-containing CRA-1 antagonizes hydrolase ACER-1 linking acetyl-CoA metabolism to the initiation of recombination during C. elegans meiosis. PLoS Genet. 11, e1005029. https://doi.org/10.1371/journal.pgen.1005029.

Garcia, V., Phelps, S.E.L., Gray, S., and Neale, M.J. (2011). Bidirectional resection of DNA double-strand breaks by Mre11 and Exo1. Nature 479, 241-244. https://doi.org/10.1038/nature10515.

Goodyer, W., Kaitna, S., Couteau, F., Ward, J.D., Boulton, S.J., and Zetka, M. (2008). HTP-3 links DSB formation with homolog pairing and crossing over during C. elegans meiosis. Dev. Cell 14, 263-274. https://doi.org/10.1016/j. devcel.2007.11.016.

Harrell, K., Day, M., and Smolikove, S. (2021). Recruitment of MRE-11 to complex DNA damage is modulated by meiosis-specific chromosome organization. Mutat. Res. 822, 111743. https://doi.org/10.1016/j.mrfmmm.2021.

Harrell, K.E., Koury, E., and Smolikove, S. (2018). Microirradiation for precise, double-strand break induction in vivo in Caenorhabditis elegans. Bio. Protoc. 8, e3130. https://doi.org/10.21769/BioProtoc.3130.

Hayashi, M., Chin, G.M., and Villeneuve, A.M. (2007). C. elegans germ cells switch between distinct modes of double-strand break repair during meiotic prophase progression. PLoS Genet. 3, e191. https://doi.org/10.1371/journal. pgen.0030191.

Hillers, K.J. (2017). Meiosis. WormBook 1-43. https://doi.org/10.1895/ wormbook.1.178.1.

Hinman, A.W., Yeh, H.-Y., Roelens, B., Yamaya, K., Woglar, A., Bourbon, H.-M.G., Chi, P., and Villeneuve, A.M. (2021). Caenorhabditis elegans DSB-3 reveals conservation and divergence among protein complexes promoting meiotic double-strand breaks. Proc. Natl. Acad. Sci. USA 118, e2109306118. https://doi.org/10.1073/pnas.2109306118.

Jagut, M., Hamminger, P., Woglar, A., Millonigg, S., Paulin, L., Mikl, M., Dello Stritto, M.R., Tang, L., Habacher, C., Tam, A., et al. (2016). Separable roles for a Caenorhabditis elegans RMI1 homolog in promoting and antagonizing meiotic crossovers ensure faithful chromosome inheritance. PLoS Biol. 14, e1002412. https://doi.org/10.1371/journal.pbio.1002412.

Janisiw, E., Dello Stritto, M.R., Jantsch, V., and Silva, N. (2018). BRCA1-BARD1 associate with the synaptonemal complex and pro-crossover factors and influence RAD-51 dynamics during Caenorhabditis elegans meiosis. PLoS Genet. 14, e1007653. https://doi.org/10.1371/journal.pgen.1007653.

Janisiw, E., Raices, M., Balmir, F., Paulin, L.F., Baudrimont, A., von Haeseler, A., Yanowitz, J.L., Jantsch, V., and Silva, N. (2020). Poly(ADP-ribose) glycohydrolase coordinates meiotic DNA double-strand break induction and repair independent of its catalytic activity. Nat. Commun. 11, 4869. https://doi.org/10. 1038/s41467-020-18693-1.

Jaramillo-Lambert, A., Ellefson, M., Villeneuve, A.M., and Engebrecht, J. (2007). Differential timing of S phases, X chromosome replication, and meiotic prophase in the C. elegans germ line. Dev. Biol. 308, 206-221. https://doi.org/ 10.1016/j.ydbio.2007.05.019.

Article



Johnson, D., Crawford, M., Cooper, T., Claeys Bouuaert, C., Keeney, S., Llorente, B., Garcia, V., and Neale, M.J. (2021). Concerted cutting by Spo11 illuminates meiotic DNA break mechanics. Nature 594, 572-576. https://doi.org/10. 1038/s41586-021-03389-3.

Joshi, N., Brown, M.S., Bishop, D.K., and Börner, G.V. (2015). Gradual implementation of the meiotic recombination program via checkpoint pathways controlled by global DSB levels. Mol. Cell 57, 797-811. https://doi.org/10. 1016/i.molcel.2014.12.027.

Kauppi, L., Barchi, M., Lange, J., Baudat, F., Jasin, M., and Keeney, S. (2013). Numerical constraints and feedback control of double-strand breaks in mouse meiosis. Genes Dev. 27, 873-886. https://doi.org/10.1101/gad.213652.113.

Keeney, S., Giroux, C.N., and Kleckner, N. (1997). Meiosis-specific DNA double-strand breaks are catalyzed by Spo11, a member of a widely conserved protein family. Cell 88, 375-384. https://doi.org/10.1016/s0092-8674(00) 81876-0.

Koury, E., Harrell, K., and Smolikove, S. (2018). Differential RPA-1 and RAD-51 recruitment in vivo throughout the C. elegans germline, as revealed by laser microirradiation. Nucleic Acids Res. 46, 748-764. https://doi.org/10.1093/nar/ gkx1243.

Lam, I., Mohibullah, N., and Keeney, S. (2017). Sequencing Spo11 oligonucleotides for mapping meiotic DNA double-strand breaks in yeast. In Meiosis, Methods in Molecular Biology, D.T. Stuart, ed. (Springer New York), pp. 51-98. https://doi.org/10.1007/978-1-4939-6340-9_3.

Lange, J., Yamada, S., Tischfield, S.E., Pan, J., Kim, S., Zhu, X., Socci, N.D., Jasin, M., and Keeney, S. (2016). The landscape of mouse meiotic doublestrand break formation, processing, and repair. Cell 167, 695-708.e16. https://doi.org/10.1016/j.cell.2016.09.035.

Lee, M.H., Han, S.M., Han, J.W., Kim, Y.M., Ahnn, J., and Koo, H.-S. (2003). Caenorhabditis elegans dna-2 is involved in DNA repair and is essential for germ-line development. FEBS Lett. 555, 250-256. https://doi.org/10.1016/ S0014-5793(03)01243-2.

Lemmens, B.B.L.G., Johnson, N.M., and Tijsterman, M. (2013). COM-1 promotes homologous recombination during Caenorhabditis elegans meiosis by antagonizing Ku-mediated non-homologous end joining. PLoS Genet. 9, e1003276. https://doi.org/10.1371/journal.pgen.1003276.

Manfrini, N., Guerini, I., Citterio, A., Lucchini, G., and Longhese, M.P. (2010). Processing of meiotic DNA double strand breaks requires cyclin-dependent Kinase and multiple nucleases. J. Biol. Chem. 285, 11628-11637. https:// doi.org/10.1074/jbc.M110.104083.

Martinez-Perez, E., Schvarzstein, M., Barroso, C., Lightfoot, J., Dernburg, A.F., and Villeneuve, A.M. (2008). Crossovers trigger a remodeling of meiotic chromosome axis composition that is linked to two-step loss of sister chromatid cohesion. Genes Dev. 22, 2886-2901. https://doi.org/10.1101/gad. 1694108.

Mets, D.G., and Meyer, B.J. (2009). Condensins regulate meiotic DNA break distribution, thus crossover frequency, by controlling chromosome structure. Cell 139, 73-86. https://doi.org/10.1016/j.cell.2009.07.035.

Murakami, H., and Keeney, S. (2008). Regulating the formation of DNA doublestrand breaks in meiosis. Genes Dev. 22, 286-292. https://doi.org/10.1101/ gad.1642308.

Paiano, J., Wu, W., Yamada, S., Sciascia, N., Callen, E., Paola Cotrim, A., Deshpande, R.A., Maman, Y., Day, A., Paull, T.T., and Nussenzweig, A. (2020). ATM and PRDM9 regulate SPO11-bound recombination intermediates during meiosis. Nat. Commun. 11, 857. https://doi.org/10.1038/s41467-020-

Paix, A., Schmidt, H., and Seydoux, G. (2016). Cas9-assisted recombineering in C. elegans: genome editing using in vivo assembly of linear DNAs. Nucleic Acids Res. 44, e128. https://doi.org/10.1093/nar/gkw502.

Pratto, F., Brick, K., Cheng, G., Lam, K.-W.G., Cloutier, J.M., Dahiya, D., Wellard, S.R., Jordan, P.W., and Camerini-Otero, R.D. (2021). Meiotic recombination mirrors patterns of germline replication in mice and humans. Cell 184, 4251-4267.e20. https://doi.org/10.1016/j.cell.2021.06.025.

Prieler, S., Chen, D., Huang, L., Mayrhofer, E., Zsótér, S., Vesely, M., Mbogning, J., and Klein, F. (2021). Spo11 generates gaps through concerted cuts at sites of topological stress. Nature 594, 577-582. https://doi.org/10.1038/ s41586-021-03632-x.

Reddy, K.C., and Villeneuve, A.M. (2004). C. elegans HIM-17 links chromatin modification and competence for initiation of meiotic recombination. Cell 118, 439-452. https://doi.org/10.1016/j.cell.2004.07.026.

Reichman, R., Shi, Z., Malone, R., and Smolikove, S. (2018). Mitotic and meiotic functions for the SUMOylation pathway in the Caenorhabditis elegans germline. Genetics 208, 1421-1441. https://doi.org/10.1534/genetics.118.

Richardson, J.M., Dawson, A., O'Hagan, N., Taylor, P., Finnegan, D.J., and Walkinshaw, M.D. (2006). Mechanism of Mos1 transposition: insights from structural analysis. EMBO J. 25, 1324-1334. https://doi.org/10.1038/sj.emboj.7601018.

Robert, V.J., Davis, M.W., Jorgensen, E.M., and Bessereau, J.-L. (2008). Gene conversion and end-joining-repair double-strand breaks in the Caenorhabditis elegans germline. Genetics 180, 673-679. https://doi.org/10.1534/genetics. 108.089698.

Roig, I., Dowdle, J.A., Toth, A., de Rooij, D.G., Jasin, M., and Keeney, S. (2010). Mouse TRIP13/PCH2 is required for recombination and normal higher-order chromosome structure during meiosis. PLoS Genet. 6, e1001062. https:// doi.org/10.1371/journal.pgen.1001062.

Romanienko, P.J., and Camerini-Otero, R.D. (2000). The mouse Spo11 gene is required for meiotic chromosome synapsis. Mol. Cell 6, 975-987. https://doi. org/10.1016/S1097-2765(00)00097-6.

Rosu, S., Libuda, D.E., and Villeneuve, A.M. (2011). Robust crossover assurance and regulated interhomolog access maintain meiotic crossover number. Science 334, 1286-1289. https://doi.org/10.1126/science.1212424.

Rosu, S., Zawadzki, K.A., Stamper, E.L., Libuda, D.E., Reese, A.L., Dernburg, A.F., and Villeneuve, A.M. (2013). The C. elegans DSB-2 protein reveals a regulatory network that controls competence for meiotic DSB formation and promotes crossover assurance. PLoS Genet. 9, e1003674. https://doi.org/10. 1371/journal.pgen.1003674.

Sanchez-Moran, E., Santos, J.-L., Jones, G.H., and Franklin, F.C.H. (2007). ASY1 mediates AtDMC1-dependent interhomolog recombination during meiosis in Arabidopsis. Genes Dev. 21, 2220-2233. https://doi.org/10.1101/ gad.439007.

Sandhu, R., Monge Neria, F., Monge Neria, J., Chen, X., Hollingsworth, N.M., and Börner, G.V. (2020). DNA helicase Mph1FANCM ensures meiotic recombination between parental chromosomes by dissociating precocious displacement loops. Dev. Cell 53, 458-472.e5. https://doi.org/10.1016/j.devcel.2020.04.010.

Stamper, E.L., Rodenbusch, S.E., Rosu, S., Ahringer, J., Villeneuve, A.M., and Dernburg, A.F. (2013). Identification of DSB-1, a protein required for initiation of meiotic recombination in Caenorhabditis elegans, illuminates a crossover assurance checkpoint. PLoS Genet. 9, e1003679. https://doi.org/10.1371/ journal.pgen.1003679.

Stracker, T.H., and Petrini, J.H.J. (2011). The MRE11 complex: starting from the ends. Nat. Rev. Mol. Cell Biol. 12, 90-103. https://doi.org/10.1038/

Thacker, D., Mohibullah, N., Zhu, X., and Keeney, S. (2014). Homologue engagement controls meiotic DNA break number and distribution. Nature 510, 241-246. https://doi.org/10.1038/nature13120.

Tolkin, T., and Hubbard, E.J.A. (2021). Germline stem and progenitor cell aging in C. elegans. Front. Cell Dev. Biol. 9, 699671. https://doi.org/10.3389/fcell.

Vrielynck, N., Schneider, K., Rodriguez, M., Sims, J., Chambon, A., Hurel, A., De Muyt, A., Ronceret, A., Krsicka, O., Mézard, C., et al. (2021). Conservation and divergence of meiotic DNA double strand break forming mechanisms in Arabidopsis thaliana. Nucleic Acids Res., gkab715. https://doi.org/10.1093/ nar/gkab715.





Wagner, C.R., Kuervers, L., Baillie, D.L., and Yanowitz, J.L. (2010). xnd-1 regulates the global recombination landscape in Caenorhabditis elegans. Nature 467, 839-843. https://doi.org/10.1038/nature09429.

Woglar, A., Daryabeigi, A., Adamo, A., Habacher, C., Machacek, T., La Volpe, A., and Jantsch, V. (2013). Matefin/SUN-1 phosphorylation is part of a surveillance mechanism to coordinate chromosome synapsis and recombination with meiotic progression and chromosome movement. PLoS Genet. 9, e1003335. https://doi.org/10.1371/journal.pgen.1003335.

Yamada, S., Hinch, A.G., Kamido, H., Zhang, Y., Edelmann, W., and Keeney, S. (2020). Molecular structures and mechanisms of DNA break processing in mouse meiosis. Genes Dev. 34, 806-818. https://doi.org/10.1101/gad. 336032.119.

Yin, Y., and Smolikove, S. (2013). Impaired resection of meiotic double-strand breaks channels repair to nonhomologous end joining in Caenorhabditis elegans. Mol. Cell Biol. 33, 2732-2747. https://doi.org/10.1128/MCB.00055-13.

Yokoo, R., Zawadzki, K.A., Nabeshima, K., Drake, M., Arur, S., and Villeneuve, A.M. (2012). COSA-1 reveals robust homeostasis and separable licensing and reinforcement steps governing meiotic crossovers. Cell 149, 75-87. https:// doi.org/10.1016/j.cell.2012.01.052.

Zakharyevich, K., Ma, Y., Tang, S., Hwang, P.Y.-H., Boiteux, S., and Hunter, N. (2010). Temporally and biochemically distinct activities of Exo1 during meiosis: double-strand break resection and resolution of double holliday junctions. Mol. Cell 40, 1001-1015. https://doi.org/10.1016/j.molcel.2010.11.032.

Zhang, L., Köhler, S., Rillo-Bohn, R., and Dernburg, A.F. (2018). A compartmentalized signaling network mediates crossover control in meiosis. Elife 7, e30789. https://doi.org/10.7554/eLife.30789.

Zhang, L., Ward, J.D., Cheng, Z., and Dernburg, A.F. (2015). The auxin-inducible degradation (AID) system enables versatile conditional protein depletion in C. elegans. Development 142, 4374-4384. https://doi.org/10.1242/dev. 129635.

Zickler, D., and Kleckner, N. (2015). Recombination, pairing, and synapsis of homologs during meiosis. Cold Spring Harb. Perspect. Biol. 7, a016626. https://doi.org/10.1101/cshperspect.a016626.

Zickler, D., and Kleckner, N. (1999). Meiotic chromosomes: integrating structure and function. Annu. Rev. Genet. 33, 603-754. https://doi.org/10.1146/annurev.genet.33.1.603.

Cell Reports Article



STAR***METHODS**

KEY RESOURCES TABLE

REAGENT or RESOURCE	SOURCE	IDENTIFIER	
Antibodies			
Monoclonal mouse anti-FLAG M2 (1:1,000)	Sigma	Cat. # F1804; RRID:AB_262044	
Polyclonal rabbit anti-HA (1:1,000)	Sigma	Cat. # H6908; RRID:AB_260070	
Polyclonal rabbit anti-OLLAS (1:1,500)	Genscript	Cat. # A01658; RRID:AB_2622186	
Monoclonal rat anti-OLLAS (1:500)	Thermofisher	Cat. # MA5-16125 (RRID code unavailable	
Polyclonal rabbit anti-SYP-1 (1:1,000)	Silva lab	(Janisiw et al., 2020)	
Polyclonal rat anti-SYP-1 (1:100)	Silva lab	This study	
Polyclonal chicken anti-RAD-51 (1:1,000)	Libuda lab	Libuda Lab	
Polyclonal rabbit anti-HTP-1 (1:400)	Martinez-Perez lab	Martinez-Perez lab	
Polyclonal rabbit anti-RAD-51 (1:30,000)	Smolikove lab	Smolikove lab	
Polyclonal guinea pig anti-phosphorylated SUN-1 ^{S8} (1:750)	Jantsch lab	(Woglar et al., 2013)	
Goat anti-rabbit Alexa Fluor 488 (1:500)	Thermofisher	Cat. # A32731; RRID:AB_2633280	
Goat anti-rabbit Alexa Fluor 594 (1:500)	Thermofisher	Cat. # A-11037; RRID:AB_2534095	
Goat anti-mouse Alexa Fluor 488 (1:500)	Thermofisher	Cat. # A-11029; RRID:AB_2534088	
Goat anti-mouse Alexa Fluor 594 (1:500)	Thermofisher	Cat. # A-11032; RRID:AB_2534091	
Goat anti-rat Alexa Fluor 488 (1:500)	Thermofisher	Cat. # A-11006; RRID:AB_2534074	
Goat anti-rat Alexa Fluor 594 (1:500)	Thermofisher	Cat. # A-11007; RRID:AB_10561522	
Goat anti-mouse HRP (1:8,000)	Thermofisher	Cat. # 31430 (RRID code unavailable)	
Donkey anti-mouse AlexaFluor 488 (1:500)	Thermofisher	Cat. # A-21202; RRID:AB_141607	
Donkey anti-mouse AlexaFluor 555 (1:500)	Thermofisher	Cat. # A-31570; RRID:AB_2536180	
Donkey anti-rabbit AlexaFluor 488 (1:500)	Thermofisher	Cat. # A-21206; RRID:AB_2535792	
Bacterial and virus strains			
E. coli OP50	CGC	OP50	
Chemicals, peptides, and recombinant proteins			
Auxin	Sigma	Cat. # I3750	
4',6-Diamidine-2'-phenylindole dihydrochloride (DAPI)	Roche	Cat. #10236276001	
VECTASHIELD Antifade Mounting Medium	Vector Laboratories	Cat. # H-1000	
SYP-1 (DNFTIWVDAPTEAL IETPVDDQS)	Genscript	SYP-1	
Critical commercial assays			
Click-iT EdU Cell Proliferation Kit for Imaging, Alexa Fluor TM 555 dye	Thermofisher	Cat. # C10338	
Experimental models: Organisms/strains			
C. elegans/ mels8 II; spo-11(ie59[spo- 11::AID::3xFLAG]) ieSi38 IV.	CGC	CA1423	
C. elegans/ cosa-1(ddr12[OLLAS::cosa-1]) III.	Silva lab	NSV97	
C. elegans/ rmh-1(jf172 [HA::rmh-1]) I.	Silva lab	NSV240	
C. elegans/ msh-5[ddr22(GFP::msh-5)] IV.	Silva lab	NSV129	
C. elegans/ OLLAS::cosa-1 III; spo- 11::AID::3xFLAG ieSi38 IV.	Silva lab	NSV420	
C. elegans/ spo-11(ddr35[spo-11::HA)] IV.	Silva lab	NSV192	
· · · ·		(Continued on next page)	

(Continued on next page)





Continued				
REAGENT or RESOURCE	SOURCE	IDENTIFIER		
C. elegans/ HA::rmh-1 I; OLLAS::cosa-1 III; spo-11::AID::3xFLAG ie Si38 IV.	Silva lab	NSV435		
C. elegans/ brc-1(ddr6[brc-1::HA)] III.	Silva lab	NSV49		
C. elegans/ syp-3(iow69[3xFLAG::syp-3]) I	Smolikove lab	SSM428		
C. elegans/ dna-2(iow111[dna- 2::degron::3XFLAG]) II; unc-119(ed3) III; ieSi38 [sun-1p::TIR1::mRuby::sun-1 3'UTR + Cbr-unc-119(+)] IV.	Smolikove lab	SSM540		
C. elegans/ dna-2(iow111[dna- 2::degron::3XFLAG]) II; exo-1(iow56[exo- 1::flag::GFP])]); unc-119(ed3) III; ieSi38 [sun-1p::TIR1::mRuby::sun-1 3'UTR + Cbr- unc-119(+)] IV.	Smolikove lab	SSM603		
C. elegans/ dna-2(iow111[dna- 2::degron::3XFLAG]) II, unc-119(ed3) III; ieSi38 [sun-1p::TIR1::mRuby::sun-1 3'UTR + Cbr-unc-119(+)] IV; msh-5(me23)/ nT1 (IV,V).	Smolikove lab	SSM653		
C. elegans/ dna-2(iow111[dna- 2::degron::3XFLAG]) II, unc-119(ed3) III; ieSi38 [sun-1p::TIR1::mRuby::sun-1 3'UTR + Cbr-unc-119(+)] IV; cku- 70(tm1524) exo-1(tm1842) III.	Smolikove lab	SSM643		
C. elegans/ exo-1(iow56[exo-1 ::flag::GFP]) III.	Smolikove lab	SSM399		
C. elegans/ dna-2(iow111[dna- 2::degron::3XFLAG]) II, unc-119(ed3)III ieSi38 [sun-1p::TIR1::mRuby::sun-1 3'UTR + Cbr-unc-119(+)] IV; gfp::cku- 80(jf150) exo-1(tm1842) III	Smolikove lab	SSM590		
C. elegans/ cku-80(jf150[gfp::cku-80]) III	CGC	UV159		
Wistar Rat	Genscript	N/A		
Software and algorithms				
Photoshop	Adobe	N/A		
Softworx	AppliedPrecision	N/A		
Office	Microscoft	N/A		
ImageJ	Fiji	N/A		
Prism	GraphPad	N/A		
MetaMorph	Molecular Devices	N/A		

RESOURCE AVAILABILITY

Lead contact

Further information and requests for resources and reagents should be directed to and will be fulfilled by the lead contact, Nicola Silva (silva@med.muni.cz).

Materials availability

Strains and reagents generated in this study will be available upon request without restrictions.

Data and code availability

- All data reported in this paper will be shared by the Lead contact upon request.
- This paper does not report original code.
- Any additional information required to reanalyse the data reported in this work is available from the Lead contact upon request.



EXPERIMENTAL MODEL AND SUBJECT DETAILS

Worm lines

All C. elegans strains employed in this study were maintained following standard conditions on NG medium plates at 20°C. Animals were picked as L4 or young adult stage depending on the specific experimental requirements. The genotype of all mutant alleles and tagged lines used in this study are reported in the key resources table.

Bacterial strains

E. coli OP50 strain (uracil auxotroph) was used as food source for C. elegans strains.

Rats

Wistar Rats were employed for the generation of the anti-SYP-1 antibody, whose handling and maintenance were carried out by Genscript (https://www.genscript.com/) following standard procedures.

METHOD DETAILS

C. elegans genetics

The strains were grown according to standard procedures (Brenner, 1974). The N2 Bristol was used as wild-type control animals and worms were grown at 20°C for all experiments.

Auxin treatment

In Figure 1, worms of the indicated genotype and age were picked on NGM plates containing 1mM 3-Indoleacetic acid (Auxin) dissolved in absolute ethanol and maintained at 20°C for the specified times with minimal light exposure. For exposures in Figures 2A and S1, worms were picked as synchronized young adults, and as L4s in Figures 2B, S2A, S2B, 3, and 4. For auxin exposure in Figures 5, 6, 7, S5C, and S6 synchronized young adults were used. Control plates (-auxin) were prepared in the same way by adding an equal volume of absolute ethanol without auxin. For experiments in Figure S3B, worms were maintained on auxin plates for 48h without exposure to IR or irradiated with 10 Gy after 24h of auxin-induced depletion and left on auxin-containing plates for further 24h. In recovery experiments in Figures 7A and 7B, worms were picked to auxin plates as described above and transferred to NGM plates for 24h recovery.

Generation of SYP-1 antibody

The synthetic peptide "DNFTIWVDAPTEALIETPVDDQS" corresponding to the N-ter of C. elegans SYP-1 was used to immunize three Rats according to standard procedures (Genscript). After four rounds of immunization, the raw serum from each animal was pooled and affinity purified. Specificity of the antibody was assessed by immunofluorescence in WT worms subjected to syp-1^{RNAi} in which, unlike in the untreated animals, SYP-1 loading was largely absent.

Antibody staining

Worms were picked at L4 stage 20-24h prior to dissections unless otherwise indicated. For immunofluorescence, animals were dissected in 1x PBS and fixed at room temperature for 5' by adding an equal volume of 2% PFA diluted in 1x PBS except in Figures 5, 6, 7G, 7H, S5B, S5C, S6. In these experiments, dissection was performed in sperm salts and fixed at room temperature for 5' by adding an equal volume of 4% PFA diluted in 1X PBS. Slides were freeze-cracked in liquid nitrogen and immediately placed in methanol at -20°C for at least 5'. For staining in Figures 5, 6, 7, and S4B-C, slides were flash frozen on dry ice and dipped in methanol at -20°C for 2' and acetone at -20°C for 10s. Washes were performed in 1x PBS with 0.1% Tween (1xPBST) and blocked in 1% BSA dissolved in 1xPBST. In Figures 6, 7, S5D-F and S5I, S6 where a GFP-tagged line was dissected and imaged, no block or primary antibody was applied. Incubation of primary antibodies was conducted over night at 4°C and the day after, three washes in 1xPBST were performed before applying secondary antibodies for 2h at room temperature in the dark. Chromatin was counterstained with 60μl of 4',6-diamidino-2-phenylindole (DAPI, Roche, 2ng/ml) for 1', except in Figures 5, 6, 7, and S4B-S6 where a 1:10,000 dilution of 5mg/mL DAPI stock (Sigma) in 1X PBST was used and slides were incubated for 10' at room temperature in the dark. Slides were washed in 1xPBST for 20'at room temperature in the dark. Slides were mounted in Vectashield and coverslips were sealed with nail polish.

Image acquisition

Samples were in all but Figures 5, 6, 7, and S4B-S6 imaged with an Upright fluorescence microscope Zeiss Axiolmager.Z2-ZEN with an Apochromat 100x /1.40 OIL and z-stacks were set at 0.24 μm thickness. Images were then deconvolved with Zen Blue software using the constrained iterative algorithm set with "maximum strength." Full projections of deconvolved images were done in Fiji and further processed in Photoshop, where some false coloring was applied.

Samples in Figures 5, 6, 7, S5, S6A, and S6B were imaged on a DeltaVision wide-field fluorescence microscope (GE Lifesciences) with 100X/1.4 NA oil Olympus objective and z-stacks set at 0.2 μm thickness. Images were deconvolved (using conservative ratio





setting) and analyzed with softWoRx software (Applied Precision). Whole germline images in Figures 6C and E were taken on a Leica DMi8 platform live-cell microscope at the 20X objective with z-stacks set at 1μm thickness.

For quantification of OLLAS:COSA-1 foci, the last seven rows of nuclei prior diplotene entry were used; for HA::RMH-1 and RAD-51 foci counts, quantification was performed as in (Janisiw et al., 2020). Number of nuclei analysed for OLLAS::COSA-1, HA::RMH-1 and RAD-51 are reported in the Table S1.

For quantification of phospho-SUN-1^{S8} staining, gonads were divided into 5 equal regions spanning the transition zone to the pachytene exit. All nuclei in each region were counted and the % of positive nuclei/all nuclei was calculated.

Ethanol fixation

For experiments in Figures 6D, 6G, 7A-7F, S5D, E, F, I and S6, and S6E worms were picked as L4s and grown on NGM plates at 20°C for 18-20h. Worms were then placed on an uncharged slide (Surgipath Leica) in a drop of M9 buffer and M9 was removed with Whatman filter paper. Worms were then fixed with 8μL absolute ethanol, mounted with Vectashield+DAPI, and coverslips were sealed with nail polish for imaging.

Western blot

To produce whole cell extracts, 200 worms at L4 stage of the untagged WT and dna-2::AID::3xFLAG backgrounds were selected and 20h later they were placed onto auxin-containing plates and – auxin plates for 4h. Worms were then picked in 1x TE buffer (10mM Tris, 1mM EDTA pH 8) containing 1x protease inhibitor cocktail (Roche), snap frozen in liquid nitrogen twice and then an equal amount of 2x Laemmli Buffer was added. Samples were boiled for 10', spun for 30''at maximum speed and fully loaded on a 4%-20% precast acrylamide gel (BioRad). Protein transfer was performed onto a nitrocellulose membrane for 90' at 4°C and blocking was performed in 5% BSA in 1xTBST (1xTBS buffer with 0.1% Tween). Primary antibodies were diluted in the blocking buffer and left to probe the membrane over night at 4°C. The following day, the membrane was washed extensively in 1xTBST, secondary antibodies were diluted in 5% milk dissolved in 1xTBST and left to incubate for 60' at room temperature. After removing the secondary antibodies, the blots were extensively washed in 1xTBST and Clarity Max ECL (BioRad) was employed for detection of proteins by chemiluminescence with a G:Box (Syngene).

UV laser microirradiation

The protocol outlined in (Harrell et al., 2018) for microirradiation of whole, live worms with recovery was used in Figures 6F, 6G, and S6I. Worms were recovered to NGM plates for the notated time periods before fixation and imaging with the DeltaVision microscope. In all microirradiation experiments, at least four worms were subjected to laser in both gonad arms and subsequent analysis. Analysis and deconvolution were performed in softWoRx software. DNA-2::FLAG foci in Figures 6F and S5I were counted in at least three gonads for each condition listed and the number of microirradiated nuclei analysed were 18 (PMT 12min recovery), 30 (PMT 2h recovery), 42 (PMT 4h recovery), 18 (EP 12min recovery), 30 (EP 2h recovery), 30 (EP 4h recovery), 18 (MP 12min recovery), 18 (MP 4h recovery), 18 (LP 12min recovery), 30 (LP 2h recovery), and 36 (LP 4h recovery). Worms in Figure 6G were fixed at the indicated times by ethanol fixation. The number of laser-targeted EXO-1::GFP nuclei analysed was 18 (PMT 12min recovery), 24 (PMT 2h recovery), 24 (PMT 4h recovery), 18 (EP 12min recovery), 24 (EP 2h recovery), 24 (EP 4h recovery), 18 (MP 12min recovery), 18 (MP 4h recovery), 24 (LP 12min recovery), 24 (LP 2h recovery), and 24 (LP 4h recovery).

Fluorescence intensity

Measurements and analysis of nuclear fluorescence intensity in Figures 5C, 6B, 6D, 6H, 7G, S5 and S6 were performed using FIJI ImageJ software without deconvolution. All intensity measurements were calculated against average nuclear (Figure 5C) or cytoplasmic (6B, 6D, 6H, 7G, S7B-H) backgrounds and at least three germlines were analysed in each instance.

For RAD-51 focus intensity in Figure 5C, reported measurements were corrected against the average nuclear background and the number of foci measured was 87 (wild type), 66 (dna-2::AID), and 19 (dna-2::AID;exo-1).

For quantification of protein localization, the fluorescence intensity of the nucleus was taken and corrected against the average cytoplasmic background. The number of nuclei analysed were 23 (PMT), 18 (TZ), 23 (MP), 19 (LP) in Figure 6B and 33 (PMT), 40 (TZ), 38 (MP), 28 (LP) in Figure 3E and 33 (PMT), 40 (TZ), 37 (MP), and 28 (LP) in Figure 6C.

In Figure 7G, 37 (PMT), 26 (PMT +auxin), 48 (TZ), 51 (TZ +auxin), 45 (MP), 59 (MP +auxin), 38 (LP), and 51 (LP +auxin) nuclei were measured.

Wild-type nuclear fluorescence intensity measurements in Figures S5C and S5E are the same data points presented in Figures 6B and 6D. For measurements in dna-2::AID::3XFLAG;exo-1 in Figure S5B, 33 (PMT), 34 (TZ), 35 (MP), and 26 (LP) nuclei were analysed. For EXO-1::GFP localization in the dna-2 background, 37 (PMT), 37 (TZ), 40 (MP), and 32 (LP) nuclei were analysed. In Figure S5G, 42 (Untagged, zone 5), 71 (no auxin, zone 5), 40 (30m auxin, zone 5), 54 (2h auxin, zone 5), 59 (4h auxin, zone 5), 38 (untagged, zone 6), 42 (no auxin, zone 6), 59 (30m auxin, zone 6), 48 (2h auxin, zone 6), and 43 (4h auxin, zone 6) nuclei were measured. Data in Figure S5H (No auxin-4h auxin) is the same as that of Figure 6H with 42 (untagged, zone 5), 59 (no auxin, zone 5), 68 (30m auxin, zone 5), 75 (2h auxin, zone 5), 68 (4h auxin, zone 5), 38 (untagged, zone 6), 80 (no auxin, zone 6), 70 (30m auxin, zone 6), 59 (2h auxin, zone 6), and 58 (4h auxin, zone 6) nuclei measured.

Cell Reports Article



For GFP::cKU-80 localization in Figure S6B, 37 (PMT), 36 (PMT +auxin), 52 (TZ), 48 (TZ +auxin), 41 (MP), 71 (MP +auxin), 44 (LP), and 45 (LP +auxin) nuclei were measured.

Meiotic progression with EdU

EdU staining was performed using the Click-iTTM EdU AlexaFluor Imaging Kit from Invitrogen. Synchronized young adults or L4s, depending on the experiment (see figure legend Figures 1 and S1), were picked into M9 buffer with an equal volume of 1mM EdU and incubated in the dark at 20°C for 15'. Worms were then recovered onto NGM plates for 15' in the dark and then moved to auxin plates for the times listed. Samples were dissected in 1X PBS and fixed with an equal volume of 7.4% PFA. Fixed slides were incubated for 10' at room temperature in the dark and then transferred to dry ice for 30'. Slides were then incubated in -20° C methanol for 20' and washed with 1X PBST 3 times for 10' each. 100μl EdU processing solution was added to each sample, covered with a Parafilm strip, and rapidly moved to incubation in the dark at room temperature for 1h. Slides were then washed with 1X PBST 3 times for 10' each and chromatin stained by incubating with a 1:10,000 dilution DAPI (5mg/ml stock) in 1X PBS for 20' in the dark. Slides were then mounted with Vectashield, and coverslips sealed with nail polish. EdU-stained gonads were imaged on the DeltaVision microscope at 20X magnification with auxiliary magnification enabled.

Quantification of meiotic progression was calculated based on the nuclear row position of the most proximal EdU-positive nuclei where at least 50% of the nuclei in the row were EdU-positive and 4 germlines were quantified.

CRISPR/Cas9 genome editing

CRISPR/Cas9 was used to generate the dna-2::degron::3xFLAG strain used in this study. Microinjection of 1-day-old adult worms was performed on 3% agarose pads and worms were subsequently recovered to individual OP50-seeded plates the following day. F1 progeny were screened for rol and dpy phenotypes generated by dpy-10 point mutation used by co-CRISPR injection marker, adopted from (Paix et al., 2016). Wild-type siblings were singled to individual plates for screening by PCR and Sanger sequencing. This microinjection was performed in two steps to accommodate size limitations in efficient CRISPR/Cas9 genome editing. tracrRNA, crRNA, and ssODN were obtained from IDT and mixed in the following concentrations: 14.35µM Cas9-NLS (Berkeley MacroLab), 17.6 μM tracr-RNA, 1.5μM dpy10 crRNA, 0.5μM dpy10 ssODN, 16.2 μM target crRNA, and 6μM target ssODN.

QUANTIFICATION AND STATISTICAL ANALYSIS

Statistical analysis was performed with GraphPad Prism by using Two-tailed Mann-Whitney test, Chi-square or two-way ANOVA depending on the experimental settings. All details regarding the statistical test employed, the size of the samples and P values are all included in the figure legends.